



DR. QING TIAN (Orcid ID : 0000-0003-2795-363X)

Article type : Original Article

Evidence of altered depression and dementia-related proteins in the brains of young rats after ovariectomy

Ying-Yan Fang^{a, b, 1}, Peng Zeng^{a, b, 1}, Na Qu^{b, c}, Lin-Na Ning^{a, b}, Jiang Chu^{a, b}, Teng Zhang^{a, b}, Xin-Wen Zhou^{a, b, *}, Qing Tian^{a, b, *}

a Department of Pathology and Pathophysiology, School of Basic Medicine, Tongji Medical College, Huazhong University of Science and Technology

b Institute for Brain Research, Huazhong University of Science and Technology

c Affiliated Mental Health Center, Tongji Medical College, Huazhong University of Science and Technology, Wuhan 430022, China

1 Equally contributed to this work.

* Corresponding authors at: Department of Pathology and Pathophysiology, School of Basic Medicine, Tongji Medical College, Huazhong University of Science and Technology, 13# Hangkong Road, Wuhan 430030, China. Tel.: +86 27 83692625; Fax: +86 27 83692608.

Email addresses: zhouxinwen@hust.edu.cn, tianq@hust.edu.cn.

This article has been accepted for publication and undergone full peer review but has not been through the copyediting, typesetting, pagination and proofreading process, which may lead to differences between this version and the Version of Record. Please cite this article as doi: 10.1111/jnc.14537

This article is protected by copyright. All rights reserved.

Abstract:

Menopause, a risk factor for brain dysfunction in women, is characterized by neuropsychological symptoms including depression and dementia, which are closely related to alterations in different brain regions after menopause. However, little is known about the variability of pathophysiologic changes associated with menopause in the brain. Here, we observed that menopause in rats induced by bilateral ovariectomy (OVX) showed depressive and dementia-related behaviors along with neuronal loss in the prefrontal cortex (PFC), hippocampus (HIP), hypothalamus (HYP) and amygdala (AMY) by Nissl staining. Meanwhile, by immunohistochemical staining, increased microglia in the HIP and AMY and increased astrocytes in the PFC, HYP and AMY were shown. By using quantitative proteomics, we identified 146 differentially expressed proteins in the brains of OVX rats, e.g., 20 in the PFC, 41 in the HIP, 17 in the HYP and 79 in the AMY, and performed further detection by Western blotting. A link between neuronal loss and apoptosis was suggested, as evidenced by increases in adenylate kinase 2 (AK2), B-cell lymphoma 2 associated X (Bax), cleaved caspase-3 and phosphorylated p53 and decreases in Huntingtin-interacting protein K (HYPK), hexokinase (HK), and phosphorylated B-cell lymphoma 2 (Bcl-2), and apoptosis might be triggered by endoplasmic reticulum stress (probed by increased glucose-regulated protein 78 (GRP78), cleaved caspase-12, phosphorylated protein kinase R (PKR)-like endoplasmic reticulum kinase (PERK), inositol-requiring enzyme-1 (IRE-1) and activating transcription factor 6 (ATF6)) and mitochondrial dysfunction (probed by increased cytochrome c and cleaved caspase-3 and decreased sideroflexin-1 (SFXN1) and NADH dehydrogenase (ubiquinone) 1 α subcomplex 11 (NDUFA11)). Activation of autophagy was also indicated by increased autophagy-related 7 (ATG7), γ -aminobutyric acid (GABA) receptor-associated protein-like 2 (GABARAPL2) and oxysterol-binding protein-related protein 1 (ORP1) and confirmed by increased microtubule-associated protein light chain 3 (LC3II/I), autophagy-related 5 (ATG5), and Beclin1 in the HIP and AMY. In the AMY, which is important in emotion, higher GABA transporter 3 (GAT3) and lower vesicular glutamate transporter 1 (VgluT1) levels indicated an imbalance between excitatory and inhibitory neurotransmission, and the increased calretinin and decreased calbindin levels suggested an adjustment of GABAergic transmission after OVX. In addition, cytoskeletal abnormalities including tau hyperphosphorylation, dysregulated Ca²⁺ signals and glutamic synaptic impairments were observed in the brains of OVX rats. Collectively, our study showed the changes in different brain regions related to depression and dementia during menopause.

Keywords: Ovariectomy; Apoptosis; Autophagy; Endoplasmic reticulum stress; Amygdala.

This article is protected by copyright. All rights reserved.

Abbreviations:

AK2, Adenylate kinase 2; HYPK, Huntingtin-interacting protein K; HK, Hexokinase; GRP78, Glucose-regulated protein 78; PERK, Protein kinase R (PKR)-like endoplasmic reticulum kinase; IRE-1, Inositol-requiring enzyme-1; ATF6, Activating transcription factor 6; SFXN1, Sideroflexin-1; NDUFA11, NADH dehydrogenase (ubiquinone) 1 α subcomplex 11; ATG7, Autophagy-related 7; GABARAPL2, γ -aminobutyric acid (GABA) receptor-associated protein-like 2; ORP1, Oxysterol-binding protein-related protein 1; SCAMP5, Secretory carrier membrane protein 5; HSPA1A, Heat shock 70 kDa protein 1A; LC3, Microtubule-associated protein light chain 3; ATG5, Autophagy-related 5; GSK3 β , Glycogen synthase kinase 3 β ; PI3K, Phosphoinositide-3-kinase; MEK, Mitogen-activated protein kinase kinase; ERK, Extracellular signal-regulated protein kinase; PLP, Myelin proteolipid protein; MAG, Myelin-associated glycoprotein; GAT1, GABA transporter 1; GAT3, GABA transporter 3; VgluT1, Vesicular glutamate transporter 1; NR2B, N-methyl-D-aspartate receptor 2B subunit; SHANK3, SH3, and multiple ankyrin repeat domains 3; GABAR-B2, GABA type B receptor subunit 2; EIF2 α , Eukaryotic initiation factor 2 α ; PKC, Protein kinase C; SEPT8, Septin-8; VAMP2, Vesicle-associated membrane protein 2; CAPS1, Calcium-dependent secretion activator 1; Syt, Synaptotagmin; AMPARs, α -amino-3-hydroxy-5-methyl-4-isoxazole propionic acid receptors; Fbxo2, F-box Only Protein 2; STIM2, Stromal interaction molecule 2; CaMKII α , α isoform of the calcium/calmodulin-dependent protein kinase II; HPCAL1, Hippocalcin-like protein 1; TRPC1, Transient receptor potential channel 1; Rac1, Ras-related C3 botulinum toxin substrate 1; UCH-L1, Ubiquitin C-terminal hydrolase-L1; ATAT1, α -tubulin N-acetyltransferase 1; Phk, Phosphorylase b kinase; ER α , Estrogen receptor α ; ER β , Estrogen receptor β ; CB, Calbindin; PV, Parvalbumin; CR, Calretinin.

Introduction

Developmental and physiological differences between sexes significantly contribute to the development of brain dysfunction (Cahill 2006). Indeed, the risks of neuropsychiatric abnormalities are much higher in women than those in men. It has been reported that women show a more robust progression of mild cognitive impairment and increased severity of clinical dementia including Alzheimer's disease (AD) (Mielke *et al.* 2014). Menopause, either naturally or medically induced, means the end of reproduction in females; it is mainly characterized clinically by headaches, irritability, insomnia, depression, hot flushes and fatigue and occurs in nearly all women at some point in life (O'Bryant *et al.* 2003). The transitional years between the reproductive stage and infertility that occurs just before

This article is protected by copyright. All rights reserved.

menopause is termed perimenopause, and postmenopause represents the years after menopause. Perimenopause starts in the fourth decade of life when the ovaries gradually produce decreased hormone levels. As a result of the hormone deficiency, postmenopausal women are at higher risk for brain dysfunction (Dalal and Agarwal, 2015). In perimenopausal women, the prevalence of depressive symptoms is higher than that in premenopausal women (Marsh *et al.* 2017). Moreover, the periods of menopausal transition and early postmenopause are associated with a 2- to 4-fold increased risk of clinically significant depressive symptoms (Gordon *et al.* 2018).

In women's health, estrogen not only plays important roles in the estrous cycle but also has a protective role in the brain. Estrogen depletion is regarded as the major basis for menopause-induced brain dysfunction (Brinton *et al.* 2015). Estrogen-based hormone replacement therapy (HRT) without cyclic progestin replacement is optimal for managing early menopausal symptoms (Sarrel *et al.* 2016). Without HRT, most menopausal women developed severe symptoms of estrogen deficiency and were at increased risk for cognitive decline, dementia, and the associated increases in morbidity and mortality (Kodaman 2010; Sarrel *et al.* 2016). It is also suggested that the outcome of HRT depends on a critical window of estrogen benefit, which relates to age at the time of treatment, type of menopause, or stage of menopause (Whitmer *et al.* 2011; Maki 2013). Estrogen influences brain function through gene transcription and rapid membrane signaling, which are mediated by estrogen receptors (ERs), including estrogen receptor α (ER α) and estrogen receptor β (ER β) (Bean *et al.* 2014). ER α and ER β are expressed in the pituitary and many brain regions, including the hypothalamus (HYP), hippocampus (HIP), amygdala (AMY), and prefrontal cortex (PFC), among others (Kuiper *et al.* 1998; Shughrue and Merchenthaler 2001; Spencer *et al.* 2008; Almey *et al.* 2015).

Previous studies support the idea that multiple factors involved in menopause induced brain damage, e.g., synapse loss, neuronal loss, blood-brain-barrier disruptions, white matter degeneration and so on (Atwood and Bowen 2015; Kantarci *et al.* 2018). Thus, considerable changes after menopause must be more rigorously considered. In this study, we established a surgical menopause rat model with an estrogen deficit induced by bilateral ovariectomy (OVX) as described previously (Qu *et al.* 2013). The OVX rats showed depressive and dementia-related behaviors. Then, we identified 146 differentially expressed proteins in the brains of OVX rats compared with sham-operated (SHAM) rats by quantitative proteomics, e.g., 20 in the PFC, 41 in the HIP, 17 in the HYP and 79 in the AMY, and performed further detection by Western blotting. By immunohistochemical staining, increased numbers of microglia in the HIP and AMY and increased numbers of astrocytes in the PFC, HYP and AMY, as well as neuronal loss in all 4 of these regions were observed by Nissl staining. It was indicated that the neuronal loss in OVX rats might be a result of apoptosis, as evidenced

by increases in adenylate kinase 2 (AK2), B-cell lymphoma 2 associated X (Bax), cleaved caspase-3 and phosphorylated p53 and decreases in Huntingtin-interacting protein K (HYPK), hexokinase (HK), and phosphorylated B-cell lymphoma 2 (Bcl-2). Increased levels of glucose-regulated protein 78 (GRP78), phosphorylated PKR-like ER kinase (PERK), inositol-requiring enzyme-1 (IRE-1), activating transcription factor 6 (ATF6), and cleaved caspase-12 marked endoplasmic reticulum (ER) stress activation. In the HIP of OVX rats, increased cytochrome c and decreased sideroflexin-1 (SFXN1), NADH dehydrogenase (ubiquinone) 1 α subcomplex 11 (NDUFA11) and HK, which suggested mitochondrial dysfunction, were observed. These data supported a strong relation between apoptosis, ER stress and mitochondrial dysfunction. Dysregulation of autophagy in the brains of OVX rats was indicated by alteration of specific autophagy-related markers/regulators, including increased levels of autophagy-related 7 (ATG7), ATG5, microtubule-associated protein light chain 3 (LC3II/I), Beclin1, γ -aminobutyric acid receptor-associated protein-like 2 (GABARAPL2), and oxysterol-binding protein-related protein 1 (ORP1) and decreased levels of secretory carrier membrane protein 5 (SCAMP5), heat shock 70 kDa protein 1A (HSPA1A) and HYPK. Synaptic impairments, especially glutamic synaptic dysfunction, were observed and might involve the dysregulation of Ca²⁺-related signals, e.g., Ras/Raf1/mitogen-activated protein kinase kinase (MEK)/extracellular signal-regulated protein kinase (ERK) (Ras/Raf1/MEK/ERK) and phosphoinositide-3-kinase/protein kinase B (PI3K/AKT) pathways. In the AMY, dysregulation of excitatory and inhibitory neurotransmission was indicated by higher GABA transporter 3 (GAT3) levels and lower vesicular glutamate transporter 1 (VgluT1) levels. The decreased phosphorylation of N-methyl-D-aspartate receptor 2B subunit (NR2B) at Y1472, Fyn and SHANK3 (SH3, and multiple ankyrin repeat domains 3) suggested dysregulation of excitatory synapses. In addition, the adjustment of GABAergic transmission in the AMY was suggested by increased levels of calretinin, decreased levels of calbindin and decreased levels of GABA type B receptor subunit 2 (GABAR-B2). Cytoskeletal abnormalities, especially tau hyperphosphorylation with glycogen synthase kinase 3 β (GSK3 β) activation, were observed in the OVX rats. Decreased levels of myelin proteolipid protein (PLP) in the HIP and HYP and decreased levels of myelin-associated glycoprotein (MAG) in the AMY indicated injury of the myelin and dysfunction of oligodendrocytes. Our study here presented the changes in different brain regions in depression and dementia after menopause.

Materials and Methods

Animals

Three-month-old female Sprague-Dawley (SD) rats (No. 42009800001739; Research Resource Identifier (RRID): RGD_70508) weighing 230-280 g each were supplied by the Experimental Animal Center of Tongji Medical College, Huazhong University of Science

This article is protected by copyright. All rights reserved.

and Technology. Rats were kept in cages under a 12 h light/12 h dark cycle (7:00 AM-7:00 PM). Rats were allowed free access to standard laboratory food and water and maintained at a constant temperature of 24 ± 2 °C. All animal experimental protocols and animal manipulation in this research were approved by the Animal Care and Use Committee of Huazhong University of Science and Technology (No. 2015042901739). This study was not pre-registered.

By using a computer randomization table (from 1 to 36, each number corresponded to a single EXCL random number, and then the two columns of numbers were sorted in descending order), 36 rats were randomly divided into 2 groups, SHAM rats (n = 18) and OVX rats (n = 18). After anesthetization with 80 mg/kg ketamine (Jiangsu Hengrui Pharmaceutical Co., Ltd., Jiangsu, China; Cat# H32022820) and 5 mg/kg xylazine (Selleck Chemicals, Houston, Texas, USA; Cat# S2516), the OVX rats were underwent bilateral ovariectomy. SHAM rats received the same incisions and sutures, but the ovaries were palpated instead of removed.

At different time points after the operation (Fig. 1), rats were subjected to the sucrose preference test (SPT), open field test (OFT), forced swimming test (FST) and Morris water maze test (MWMT). Samples were taken after the MWMT.

Rats and samples were provided to the experimenters according to the number of the rat, and the experimenters did not know the grouping of the rats. Experimenters were blinded in the behavioral tests, Western blotting, serum 17β -estradiol assay, morphological detections and proteomic analysis.

Behavioral tests

The SPT was prepared and carried out as previously described (Ning *et al.* 2018). After 24 h of food and water deprivation, rats were allowed free access to two bottles of liquid for 1 h, one bottle containing water and the other containing 1.5% sucrose. Both bottles were weighed at the beginning of the test and then weighed again 1 h later. The sucrose preference was calculated according to the ratio of sucrose consumption / (water consumption + sucrose consumption) \times 100%.

The OFT was employed to assess locomotor activity and exploration in a novel environment (Ning *et al.* 2018). The open field arena consisted of an open rectangular plastic box (100 cm \times 100 cm \times 40 cm). The floor was divided by lines into 25 equal squares (20 cm \times 20 cm) including 16 peripheral squares and 9 central squares. The rat was placed in the center square of the field and allowed to explore the area freely for 5 min. The total number of squares crossed in the arena and the number of vertical activity events were recorded. The behaviors were automatically recorded by a computer-based infrared radiation (IR) color universal

This article is protected by copyright. All rights reserved.

serial bus (USB) camera tracking system (PA-501, Gobon Electron Co., Ltd., Shenzhen, China) and analyzed by AVTAS version 3.3 software (Wuhan YiHong Science & Technology Co., Ltd., Wuhan, China).

The FST was carried out in a transparent Plexiglas cylinder (30 cm diameter × 40 cm height) containing water (25 ± 2 °C) to a depth of 25 cm from which there was no escape. During testing, the rat was forced to swim in the cylinder for 5 min, and the immobility time was recorded to assess desperation (Ning *et al.* 2018). The duration of immobile posture was considered the immobility time. The cylinder was emptied and refilled with water between rats. The behaviors were automatically recorded by a computer-based IR color USB camera tracking system (PA-501, Gobon Electron Co., Ltd., China) and analyzed by AniLab version 5.0 software (AniLab Software & Instruments Co., Ltd., Ningbo, China).

After the FST, all rats underwent a 6-day training period of spatial learning in the Morris water maze as previously described (Zhu *et al.* 2017). We filled a 1.8 meter-diameter swimming pool with black, nontoxic ink water. Room temperature was maintained at 25 °C. In the first day of training, rats were allowed to rest on the platform for 30 s and given 60 s to find the hidden platform. In cases when a rat did not find the platform within 60 s, we guided it to find and stay on the platform for 30 s. On the next day after the end of the training session, the memory abilities of all rats were tested. The behaviors were automatically recorded by a computer-based IR color USB camera tracking system (PA-501, Gobon Electron Co., Ltd., China) and analyzed by AVTAS version 4.0 software (Wuhan YiHong Science & Technology Co., Ltd., China).

Western blotting

Western blotting was performed as previously described (Ning *et al.* 2018). Tissues from the HIP and AMY were sliced and digested in buffer solution containing 10 mM Tris-HCl (pH 7.4), 50 mM NaCl, 50 mM NaF, 0.5 mM Na_3VO_4 , 1 mM EDTA, 1 mM benzamidine, 1.0 mM phenylmethylsulfonyl fluoride (PMSF), 5 mg/ml leupeptin, 5 mg/ml aprotinin, and 2 mg/ml pepstatin. Then, one-third of the extracting buffer containing 200 mM Tris-Cl (pH 7.6), 8% SDS, and 40% glycerol was added to one volume of the tissue homogenate. Lastly, the homogenates were boiled for 10 min in a water bath, ultrasonically processed for 15 s, and then stored at -80 °C. Protein concentrations were measured by using a bicinchoninic acid (BCA) kit (Thermo Fisher Scientific, Waltham, MA, USA; Cat# 23225). The proteins were separated by 10% SDS-PAGE and transferred onto nitrocellulose membranes, and then the membranes were blocked with 5% nonfat milk dissolved in Tris-buffered saline (TBS) containing 50 mM Tris-HCl (pH 7.6) and 150 mM NaCl for 1 h and probed with primary antibodies (Table 1) for 18 h. The membranes were washed with TBS-Tween-20 and incubated with anti-rabbit or anti-mouse IgG conjugated to IRDye® 800 CW (1:10,000,

Li-Cor Bioscience, Lincoln, NE, USA; RRID: AB_621842; Cat# 926-32210; RRID: AB_621843; Cat# 926-32211) for 1 h at room temperature. After washing with TBS-Tween-20, the membranes were visualized and quantitatively analyzed by an Odyssey Infrared Imager System (Li-Cor Bioscience).

Serum 17 β -estradiol assay

Serum was prepared from peripheral blood by centrifuging at 1000 \times g for 20 min. The serum 17 β -estradiol level was analyzed as the introduction of an estradiol ELISA assay kit (Elabscience Biotechnology Co., Ltd., Wuhan, China; Cat# E-EL-0065c). The results were expressed in pg/ml, and each sample was assayed in duplicate (Qu *et al.* 2013).

Nissl staining and immunohistochemical staining

The sections of brain in both groups of rats were collected consecutively for Nissl staining and immunohistochemistry as previously described (Qu *et al.* 2013; Qu *et al.* 2016). The rats were deeply anesthetized and transcardially perfused with 500 ml ice-cold PBS followed by 500 ml ice-cold 4% paraformaldehyde (PFA) in PBS. The brains were postfixed overnight in 4% PFA in PBS. Then, each brain was sliced into coronal sections (25 μ m thick) with a vibratome (VT1000S, Leica, Germany). For Nissl staining, sections were stained in 0.1% toluidine blue solution for 20 min, quickly rinsed in distilled water and differentiated in 95% ethyl alcohol for 15 min. For immunohistochemistry, the sections were blocked in 3% BSA in PBS containing 0.1% Triton X-100 and 0.3% H₂O₂ at room temperature for 30 min and then incubated with the primary antibodies (Table 1) at 4 $^{\circ}$ C in 0.1 M PBS with 3% BSA overnight. Thereafter, the sections were washed with buffer followed by incubation with secondary biotinylated goat anti-rabbit or goat anti-mouse antibodies at a dilution of 1:200 in PBS for 1 h at 37 $^{\circ}$ C. After being washed, the sections were incubated with ABC kits (Vector Laboratories, Inc., Burlingame, CA, USA; RRID: AB_2336810; Cat# PK-4001; RRID: AB_2336811, Cat# PK-4002) for 1 h at 37 $^{\circ}$ C and rinsed in buffer. Finally, after DAB incubation, the sections were washed briefly with distilled water, dehydrated in graded alcohols and cleared in xylene. The images from Nissl staining and immunohistochemical staining were captured by a virtual slide system (VSS: VS120-S6-W, Olympus, Tokyo, Japan) and analyzed with an Image-Pro Plus 6.0 system (Media Cybernetics Inc., USA).

Proteomic analysis

An integrated approach involving isobaric tags for relative and absolute quantification (iTRAQ) labeling, high-performance liquid chromatography (HPLC) fractionation and mass spectrometry-based quantitative proteomics to quantify dynamic changes in the whole proteome of rat brain tissue was used as previously described (Ning *et al.* 2018). The proteins in the PFC, HIP, HYP, and AMY samples were extracted, concentrated, and digested with

This article is protected by copyright. All rights reserved.

trypsin. Then, the obtained peptides were labeled with iTRAQ-8plex reagents in accordance with the manufacturer's protocol. The efficiency of iTRAQ labeling was above 96%. After being labeled, the peptides were fractionated by high-pH reversed-phase HPLC. For high-performance liquid chromatography/tandem mass spectrometry (LC-MS/MS) analysis, the peptides were dissolved in 0.1% formic acid (FA), loaded onto a reversed-phase precolumn (Acclaim PepMap 100, Thermo Fisher Scientific), and then separated using a reversed-phase analytical column (Acclaim PepMap RSLC, Thermo Fisher Scientific). The resulting peptides were analyzed through a Q Exactive™ Plus hybrid quadrupole-Orbitrap mass spectrometer (Thermo Fisher Scientific). To identify and quantify proteins, the resulting MS/MS data were analyzed by MaxQuant with an integrated Andromeda search engine (v.1.4.1.2), and tandem mass spectra were searched against the Uniprot_rat database (32,983 sequences). As reported, we defined observed proteins with iTRAQ ratios of > 1.30 or < 0.77 coupled with $p < 0.05$ as differentially expressed (Jiang *et al.* 2015). Cerebral cell type analyses of differentially expressed proteins were based on data of RNA cell type markers (Zhang *et al.* 2014), protein cell type markers (Sharma *et al.* 2015) and PubMed.

To investigate the differentially expressed proteins, we used Gene Ontology (GO) annotations including biological process, cellular compartment, and molecular function. For biological processes, two-tailed Fisher's exact test was used to test the enrichment of the differential expression protein against all identified proteins. The GO with a corrected $p < 0.05$ was considered significant. We sorted out all the protein groups obtained after functional enrichment analysis along with their p values and then filtered for those categories that were at least enriched in one of the protein groups with $p < 0.05$. This filtered p matrix was transformed by $-\log_{10}(p)$ (Ning *et al.* 2018).

Statistical analysis

Sample size calculations were performed using G*power version 3.1.9.2 software (Franz Faul, Uni Kiel, Germany). Differences between two independent means (two groups) in statistical tests, the α err prob = 0.05, power (1- β err prob) = 0.95, and allocation ratio $N_2/N_1 = 1$ were determined and then calculated. This allowed us to obtain the sample size of group 1 = 18, the sample size of group 2 = 18, and the total sample size = 36. The data from behavioral tests, Western blotting and morphological studies were analyzed using SPSS 12.0 (SPSS Inc., Chicago, IL, USA), and the statistical graphs were produced by GraphPad Prism (GraphPad Software, Inc., La Jolla, CA) and Microsoft Excel 2010 (Microsoft Corporation, Redmond, WA, USA). Data are expressed as the means \pm SEM. An independent-samples T test was used to determine the differences between groups. The level of significance was set at $p < 0.05$.

Results

OVX rats showed depressive behavior and cognitive impairments

In this research, the OFT, SPT, FST and MWMT were used to detect the behaviors of the rats after surgery. In the OFT performed from the 2nd to 7th week after surgery (Fig. 1), the OVX rats showed decreases in the number of rearing responses (7.00 ± 3.71) (Fig. 2a), moving duration (111.44 ± 46.67 s) (Fig. 2b) and total distance (1967.60 ± 918.15 cm) (Fig. 2c), and a decrease in the number of zone crossings (60.67 ± 30.04) after the 4th week (Fig. 2d). In the SPT, performed in the 7th week after surgery, the percentage of sugar consumption of OVX rats was $64.94 \pm 12.06\%$, which was significantly lower than that of SHAM rats ($82.90 \pm 8.81\%$) (Fig. 2e). In the FST, the immobility time of the OVX rats within 5 mins was 135.17 ± 27.76 s, significantly longer than that of SHAM rats (62.07 ± 23.77 s) (Fig. 2f). These data indicated that OVX rats had depressive behaviors. Thereafter, in the 6-day learning stage of the MWMT, the OVX rats showed longer latencies to find the platform (Fig. 2g). In the memory test, the latencies of the first platform crossing of the OVX rats (27.25 ± 14.28 s) were significantly longer than those of the SHAM rats (13.43 ± 5.88 s) (Fig. 2h), and their annulus crossings within 60 s (2.50 ± 1.45) were significantly reduced (Fig. 2i). Additionally, OVX rats had decreased levels of 17 β -estradiol in blood (Fig. 2j) and decreased levels of ER α and ER β in brain (Fig. 2k, l, m).

Brain damage in OVX rats indicated by the proteomic data

In total, 3718 proteins were identified, and 3208 proteins were quantitatively analyzed. Using an iTRAQ ratio of > 1.3 coupled with $p < 0.05$ as the upregulated threshold and < 0.77 coupled with $p < 0.05$ as the downregulated threshold, 146 differentially expressed proteins were obtained in the OVX rats, namely, 5 upregulated and 15 downregulated proteins in the PFC, 30 upregulated and 11 downregulated proteins in the HIP, 11 upregulated and 6 downregulated proteins in the HYP, and 43 upregulated and 36 downregulated proteins in the AMY. The subcellular distributions and cell properties of these proteins are shown in Fig. 3a and Fig. 3b.

Brain damage was indicated in the OVX rats. Decreased levels of ras-related C3 botulinum toxin substrate 1 (Rac1) in the HIP (73.0%) and Rac3 in the PFC (91.9%), HIP (75.2%) and AMY (70.2%, Fig. 3c) were found in the OVX rats, both of which are important for the development of the nervous system (Corbetta *et al.* 2009). Ubiquitin C-terminal hydrolase-L1 (UCH-L1), which may prospectively act as a robust and universal marker for various forms of brain injury including AD (Öhrfelt *et al.* 2016; Wang *et al.* 2017), was increased in the HIP (133.3%, Fig. 3c). Leukemia-related protein 16 (LRP16), a crucial regulator for nuclear factor kappa-light-chain-enhancer of activated B cells (NF- κ B) activation (Shao *et al.* 2015), was increased in the HYP and AMY (Fig. 3c). In addition to increased levels of UCH-L1 (in

This article is protected by copyright. All rights reserved.

the HIP), decreased levels of S100A1 (in the HIP) and stromal interaction molecule 2 (STIM2) (in the HIP, HYP and AMY), and increased levels of γ -synuclein (SNCG, in the HYP and AMY) and ER lipid raft-associated protein 2 (Erlin-2, in the HIP) also indicated AD-associated damages in the OVX rats (Fig. 3c). There were also some protective factors activated after OVX. For example, hepatoma-derived growth factor-related protein-3 (HRP-3), which has an antiapoptotic effect (Yun *et al.* 2014), was increased to 143.9% in the AMY (Fig. 3c). In the HIP, protein kinase C (PKC) ζ levels were increased to 137.9%, while PKC δ levels were increased to 137.6% and PKC ϵ levels were decreased to 88.5% (Fig. 3c). PKC β , PKC ϵ , and PKC ζ can function as suppressors of apoptosis, whereas PKC δ is proapoptotic in function (Sun and Alkon 2012). An amyloid- β (A β) cleavage protein (Silva *et al.* 2017), transthyretin (TTR), was shown to be clearly increased in the HIP (139.1%), HYP (135.0%) and AMY (156.7%) (Fig. 3c).

Injury of myelin and dysfunction of oligodendrocytes in the OVX rats were indicated by a decrease in myelin proteolipid protein (PLP) in the HIP (89.5%) and HYP (91.0%) and myelin-associated glycoprotein (MAG) in the AMY (87.3%) (Fig. 3c). However, we also observed an increase in PLP in the AMY (133.9%), myelin basic protein (MBP) in the PFC (117.2%), neuronal membrane glycoprotein M6-b (GM6B) in the PFC (108.0%) and AMY (123.9%), and neuronal membrane glycoprotein M6-a (GM6A) in the PFC (118.5%) (Fig. 3c), which are reported to be beneficial to myelin and axons. Myelin-associated oligodendrocyte basic protein (MOBP) and myelin oligodendrocyte glycoprotein (MOG), two important myelin proteins in stabilizing the myelin sheath, showed no obvious alterations.

Myeloid-associated differentiation marker (MYADM), which controls endothelial barrier function (Aranda *et al.* 2013), was decreased in the HIP (81.2%) and HYP (89.1%) and increased in the PFC (141.0%) of the OVX rats (Fig. 3c). Polymerase-1 and transcript release factor (PTRF, or Cavin-1) was decreased in the AMY (76.5%) of the OVX rats (Fig. 3c), suggesting a dysfunction of the small arteries (Swärd *et al.* 2014).

Apoptosis-associated neuronal loss after OVX

Several cell death-related proteins including HYPK, HK and AK2 were included in the proteomic data. HYPK, a negative regulator of the heat shock response and apoptosis was downregulated in both the PFC (83.6% of the level in the SHAM rats) and AMY (75.9%) of the OVX rats. HK, which prevents mitochondria-mediated apoptotic cell death (Azoulay-Zohar *et al.* 2004), was downregulated in both the HIP (85.8% of the level in the SHAM rats) and HYP (75.8%) but was increased in the PFC (121.2%) and AMY (137.2%). AK2, which is released from the mitochondrial inner membrane space during neuronal apoptosis (Peng *et al.* 2012), was significantly upregulated (134.8%) in the AMY of the OVX rats (Fig. 4a). Therefore, we measured the cell numbers in the brains of the OVX rats. By Nissl staining, the numbers of neurons were found to be decreased to 26.28% in the PFC, This article is protected by copyright. All rights reserved.

10.24% in CA1, 13.06% in CA3, 18.55% in the HYP, and 18.36% in the AMY (Fig. 3d, e). Increased numbers of microglia (in the HIP and AMY) and astrocytes (in the PFC, HYP and AMY) were observed by immunohistochemical staining (Fig. 3f, g, h, i).

ER stress-triggered apoptosis was detected in the brains of the OVX rats. A specific redox homeostasis and a high luminal Ca^{2+} environment are required in the ER, whereas an imbalance might result in ER stress. STIM2, an ER-resident Ca^{2+} sensor that regulates the cytosolic and ER free Ca^{2+} concentration (Berna-Erro *et al.* 2017), was markedly reduced in the HIP (82.9%), HYP (70.6%) and AMY (79.4%) of the OVX rats (Fig. 3c). GRP78, a marker of ER stress, and PERK, IRE-1 and ATF6, three well-defined transducers activated by ER stress, were increased in the HIP and AMY (Fig. 4b, c, d). Activated PERK will phosphorylate the translation initiation factor eukaryotic initiation factor 2 α (EIF2 α) at Ser51 to reduce the protein load in the ER. Here, levels of phosphorylated PERK at Thr980 (active form) and phosphorylated EIF2 α at Ser51 were significantly increased in the HIP and AMY of the OVX rats, indicating the activation of PERK/EIF2 α (Fig. 4b, c, d). Caspase-12, a central player in ER stress-triggered apoptosis, was also shown to be increased along with its cleaved form (c-caspase-12) (Fig. 4b, c, d).

ER stress-triggered apoptosis typically proceeds in an autophagy-dependent manner. Autophagy activation was found in the brains of the OVX rats. GABARAPL2, an autophagy marker (Polletta *et al.* 2015), was upregulated in the PFC (113.1%) and AMY (137.9%). The ubiquitin-like modifier-activating enzyme ATG7, an important regulator in autophagy, was upregulated in the PFC (132.6% of the level in the SHAM rats) and HIP (136.4%). ORP1, which governs the last steps of autophagy that lead to lysosomal degradation of cytosolic material (Wijdeven *et al.* 2016), was increased to 130.9% of that of the SHAM rats in the HIP of the OVX rats. HSPA1A, a lysosomal stabilizer, was decreased in the HYP (89.8% of the level in the SHAM rats) and AMY (76.3%) (Fig. 5a). HYPK, which is reported to augment the autophagy pathway (Choudhury *et al.* 2016), was significantly decreased in the PFC (83.6% of the level in the SHAM rats) and AMY (75.9%) of the OVX rats. SCAMP5, an autophagy flux inhibitor (Yang *et al.* 2017), was downregulated in the HIP (86.8%). Furthermore, we assayed the levels of other autophagy markers including LC3II (autophagosome formation), ATG5 (autophagosome elongation), and Beclin1 (autophagosome nucleation) by Western blotting, all of which were clearly increased in the HIP and AMY (Fig. 5b, c, d).

Apoptosis triggered by mitochondrial dysfunction was also suggested in the brains of the OVX rats. SFXN1, a mitochondrial protein likely facilitating the transport of components (notably pyridoxine) required for iron utilization into and out of the mitochondria (Fowler *et al.* 2013), was decreased to 74.0% of the level in the SHAM rats in the HIP. NDUFA11, a respiratory chain protein in the mitochondrial respiratory complex I, was slightly decreased in

This article is protected by copyright. All rights reserved.

the HIP (87.2% of the level in the SHAM rats) and significantly increased in the AMY (131.9%) of the OVX rats. It was reported that downregulation of NDUFA11 disrupted the assembly of the mitochondrial respiratory complex I (Andrews *et al.* 2013). AK2, released from the mitochondrial inner membrane space during neuronal apoptosis (Peng *et al.* 2012), was slightly decreased in the HIP (79.6% of the level in the SHAM rats) and significantly increased in the AMY (134.8%) (Fig. 4a). Additionally, the translocase of outer mitochondrial membrane 6 (TOMM6), mitochondrial import receptor subunit TOM34, and mitochondrial import inner membrane translocase subunit translocase of the inner membrane 16 (TIM16) were downregulated in the OVX rats (Fig. 5a). HK, binding to the outer mitochondrial membrane and inhibiting Bax-induced cytochrome c release and apoptosis (Azoulay-Zohar *et al.* 2004) was downregulated in both the HIP (85.8% of the level in SHAM rats) and HYP (75.8%) (Fig. 4a). By Western blotting, reduced levels of Bcl-2 and increased levels of Bax, phosphorylated p53, cytochrome c, caspase-3 and cleaved caspase-3 (c-caspase-3) were observed in the HIP and AMY of the OVX rats. (Fig. 5b, c, d).

Synaptic impairments and the imbalance of excitatory/inhibitory neurotransmission

OVX rats showed synaptic impairment in their brains. In the HIP in the OVX rats, ASAP1 (Arf-GAP with SH3 domain, ANK repeat and PH domain-containing protein 1) expression was increased to 136.8% of that in SHAM rats (Fig. 6a). Its overexpression has been reported to decrease the density of spines (Jain *et al.* 2012). Brain acid-soluble protein 1 (BASP1), a neuron-enriched protein localized mainly in synaptic vesicles (Maekawa *et al.* 2013), was decreased to 62.4% in the HIP. Septin-8 (SEPT8), which controls the binding of vesicle-associated membrane protein 2 (VAMP2) to synaptophysin and participates in neurotransmitter release (Ito *et al.* 2009), was increased to 156.7% in the HIP.

Calcium-dependent secretion activator 1 (CAPS1), which stabilizes the readily releasable synaptic vesicles and thereby enhances neurotransmitter release at synapses (Shinoda *et al.* 2016), was clearly decreased in the PFC (74.5%), HIP (62.8%) and AMY (77.0%) (Fig. 6a). By Western blotting, levels of postsynaptic density protein 95 (PSD95, a postsynaptic marker) and synapsin1 (a presynaptic marker) were found to be significantly reduced in the HIP and AMY of the OVX rats. Synaptotagmin (Syt), a presynaptic calcium sensor in neurotransmitter release, was found to be decreased in the AMY (Fig. 6b, c, d).

Glutamate is the most abundant excitatory neurotransmitter, and its receptors are divided into ionotropic glutamate receptors (iGluRs) and metabotropic glutamate receptors (mGluRs). iGluRs have 4 subtypes, N-methyl-D-aspartate receptors (NMDARs), α -amino-3-hydroxy-5-methyl-4-isoxazole propionic acid receptors (AMPA receptors), kainate receptors (GluKRs), and delta receptors (GluDRs). mGluRs indirectly modulate postsynaptic ion channels, consist of G-protein coupled receptors (mGluR1-8). NMDARs comprise 5 subunits, NR1, NR2A, NR2B, NR2C, and NR2D. AMPARs comprise 4 subunits, GluR1, 2, 3, and 4. This article is protected by copyright. All rights reserved.

and 4. In this research, levels of mGluR1, mGluR2, mGluR5, GluR1, GluR3, NR1 and NR2A showed no differences between the OVX and SHAM rats (Fig. 6). Higher levels of NR2B in the PFC (105.7%) and mGluR3 in the HIP (107.4%), lower levels of mGluR4 in the PFC (86.5%), and decreased vesicular glutamate transporter 1 (VgluT1) expression in the HIP (79.2%), AMY (85.8%) and HYP (86.7%) were observed (Fig. 6a). SHANK3, a synaptic scaffolding protein interacting with the receptors, including NMDARs, mGluRs, and AMPARs (Monteiro and Feng 2017), was decreased to 70.7% in the AMY of the OVX rats (Fig. 6a). NMDARs play central roles in synaptic plasticity and mediate neurotoxicity when overstimulated. F-box only protein 2 (Fbxo2) could precisely regulate NMDARs by ubiquitination (Atkin *et al.* 2015). In the HIP of the OVX rats, Fbxo2 was increased to 133.5% of the level in the SHAM rats (Fig. 6a). Fyn, an important kinase enhancing NR2B activity by phosphorylation at Y1472 (Nygaard 2018), was clearly decreased in the AMY (74.4% of SHAM rats) (Fig. 6a). By Western blotting, it was found in the OVX rats that the levels of phosphorylated NR2B at Y1472 were decreased to 44.89% in the HIP and 29.07% in the AMY (Fig. 6b, c, d). The α isoform of calcium/calmodulin-dependent protein kinase II (CaMKII α) interacts with NR2B and is necessary for synaptic plasticity. The disruption of CaMKII/NR2B interactions at synapses decreases the phosphorylation of CaMKII α at Thr286, lowers the phosphorylation of GluR1 (a key CaMKII substrate), and produces deficits in spatial learning (Zhou *et al.* 2007). By Western blotting, we found decreases in the phosphorylation of CaMKII α and GluR1 at Ser845 in the HIP and AMY of the OVX rats (Fig. 6b, c, d). All the above data indicated abnormalities of the glutamate receptors.

The AMY is important for emotional behaviors (Sah *et al.* 2003), drug addiction (Buffalari and See 2010) and the stress response (LeDoux 1993). How the AMY responds is largely dependent on the balance between the excitatory and inhibitory inputs to its projecting neurons, and the activities of these neurons are tightly controlled by GABAergic interneurons. GABAergic interneurons comprise 3 subtypes, calbindin (CB)-positive, parvalbumin (PV)-positive and calretinin (CR)-positive (Sorvari *et al.* 1996; Muller *et al.* 2007; Woodruff and Sah 2007). In the proteomic data, the OVX rats had a higher level of CR (131.4%) and a lower level of CB (91.2%) in the AMY (Fig. 6a). Additionally, lower levels of CB and higher levels of PV α in the PFC and HIP were also shown (Fig. 5a). It is accepted that estrogen enhances glutamatergic neurotransmission and downregulates GABAergic neurotransmission (Barth *et al.* 2015). In the AMY of the OVX rats, decreased GABAR-B2 (85.5%) and increased GAT3 (119.0%) expression were shown, while GABA transporter 1 (GAT1) was increased in the HYP (124.8%) (Fig. 6a). Furthermore, VgluT1 in the AMY was decreased to 85.8% (Fig. 6a). The phosphorylation of NR2B at Y1472 was decreased to 29.07% (Fig. 6b, d), and SHANK3, a postsynaptic scaffolding protein enriched in the density of excitatory synapses, was decreased to 70.7% (Fig. 6a). These results indicated an imbalance between excitation and inhibition in the AMY.

This article is protected by copyright. All rights reserved.

In addition to a decrease in STIM2, some other Ca²⁺ signaling molecules were presented. HPCAL1, a calcium sensor protein with neuroprotective effects (Braunewell 2012), was decreased in the HIP (86.4% of the level in the SHAM rats) (Fig. 6a). CAPS1, which stabilizes the readily releasable synaptic vesicles and thereby enhances neurotransmitter release at synapses (Shinoda *et al.* 2016), was clearly decreased in the PFC (74.5%), HIP (62.8%) and AMY (77.0%) of the OVX rats. Furthermore, the levels of transient receptor potential channel 1 (TRPC1) in the HIP and AMY of the OVX rats was decreased significantly (Fig. 6b, c, d). Several signaling pathways are involved in transient calcium-mediated changes in synaptic plasticity, including calmodulin-mediated Ras-induced signaling cascades comprising the mitogen-activated protein kinase (MAPK) and PI3K signal transduction pathways. In this research, the OVX rats had lower levels of Ras and Raf1 and significantly decreased phosphorylation of MEK at Ser217/221 (p-MEK, active form) and ERK1/2 at Thr202/Thr204 (p-ERK, active form) in the HIP and AMY (Fig. 6e, f, g). Significantly decreased phosphorylation levels of AKT at Ser473 (active form) were also observed in the HIP and AMY of the OVX rats (Fig. 6b, c, d). These data indicated that the Ras/Raf1/MEK/ERK pathway and PI3K/AKT pathway were inhibited.

Impairments of the cytoskeleton in OVX rats

The stability of the cytoskeletal system is important for the function and morphology of neurons. Abnormalities of the cytoskeleton were found in the OVX rats.

Microtubule-associated protein (MAP) was decreased to 73.6% in the HIP and increased in the HYP (to 126.3%) and AMY (to 150.8%). Tubulin α -1A chain (Tuba1a) was increased to 135.0% of the level in the SHAM rats in the HIP and decreased in the HYP (to 72.1%) and AMY (to 67.4%). ATAT1, α -tubulin N-acetyltransferase 1, was increased significantly (to 131.2% of the level in the SHAM rats) in the AMY of the OVX rats. Growth factor receptor-bound protein 2 (Grb2), an important link between cellular signaling and the neuronal cytoskeleton, decreased to 75.0% in the HIP. Protein Nudcd3, which is associated with dynein-1 and dynein-2 (Asante *et al.* 2014), was decreased in the PFC, HIP, HYP and AMY (Fig. 7a). Tau, an important microtubule-associated protein, was increased in the HIP and AMY with increased phosphorylation levels at the Ser396, Ser404 and Ser198/199/202 sites (Fig. 7b, c, d). Aggregated hyperphosphorylated tau was observed in AD brains and is related to cognitive disorders. HSPA1A, which has been reported to directly inhibit tau aggregation (Patterson *et al.* 2011) and attenuate tau toxicity by maintaining tau in a soluble, nonaggregated state (Patterson *et al.* 2011; Dou *et al.* 2003), was decreased in the HYP and AMY of the OVX rats. Phosphorylase b kinase (Phk), which phosphorylates tau at Ser262 (Sironi *et al.* 1998), was significantly increased in the HIP and AMY of the OVX rats (Fig. 7a). Furthermore, we also observed the activation of GSK3 β as indicated by a decrease in its phosphorylation at Ser9 (inactive form) (Fig. 7b, c, d). Another stress-induced kinase,

c-Jun-NH₂-terminal kinase (JNK), showed no alterations in its total levels and the levels of phosphorylation at Thr183/Thr185 (active form) in the brains of the OVX rats (Fig. 7b, c, d).

Discussion

OVX is known as ‘surgical menopause’ and is accompanied by a decrease in estrogen in female rodents. Epidemiological studies suggest that, in women, reduced estrogen levels contribute to depression, sleep disturbance, irritability, anxiety, panic disorders, and cognitive dysfunction (Campbell and Whitehead 1977; Sherwin 1998). 17 β -estradiol (E2) or selective ER α agonists enhanced spatial memory (Qu *et al.* 2013; Xu *et al.* 2015), and diarylpropionitrile (DPN), an ER β -selective agonist, contributed to enhancements in recognition memory in rodents with OVX (Jacome *et al.* 2010). Hippocampal ER α and ER β activation rescued memory deficits, but only ER β activation was effective in decreasing depressive-like behavior over 12 weeks in OVX mice (Bastos *et al.* 2015). Little is known about the variability of pathologic changes in the brain after menopause, which are closely connected with the multiplicity of the clinical manifestations. Our data from the proteomic analyses and Western blotting showed the changes related to depression and dementia in the PFC, HIP, HYP and AMY after menopause.

The PFC and HIP are the brain regions most affected after OVX as reported above. As detected by a three-dimensional (3-D) reconstructed method, OVX rats with memory impairments displayed reduced brain volume in the HIP and neocortex and in the brain as a whole. In contrast, the volumes of the caudate putamen (CPU) and cerebellum of OVX rats increased slightly (Su *et al.* 2012). The CA3 neuron density in OVX rats was significantly lower, but the CA1 neuron density was significantly higher (Su *et al.* 2012). Here, we found neuronal loss in the PFC, both CA1 and CA3 in the HIP, HYP and AMY after OVX by Nissl staining. The data from the proteomic analyses and Western blotting suggested a link between neuronal loss and apoptosis, which might be triggered by ER stress and mitochondrial dysfunction after OVX. Increased numbers of microglia in the HIP and AMY and increased numbers of astrocytes in the PFC, HYP and AMY after OVX were also observed in this research by immunohistochemical staining. It was reported that lower spine densities in the pyramidal neurons of the medial PFC and the CA1 region, but not the CA3, of the HIP were shown by Golgi impregnation in OVX rats (Wallace *et al.* 2006). In our study, the levels of PSD95 (a postsynaptic marker) and synapsin1 (a presynaptic marker) were significantly reduced in the HIP and AMY of OVX rats. Dysregulated Ca²⁺ signals and glutamic synaptic impairments were observed and implicated in the synaptic impairments of the OVX rats. In the AMY, an important region in emotion, an imbalance between excitatory and inhibitory neurotransmission and an adjustment in GABAergic transmission after OVX were also indicated in this research.

The major GABA transporter GAT1 is expressed at presynaptic terminals and by astrocytes (Gadea and López-Colomé 2001), and its increase possibly results in less GABA at the synaptic cleft (Masocha 2015). Tiagabine, a selective inhibitor of GAT1, has anxiolytic-like, sedative and antidepressant-like properties (Thoeringer *et al.* 2010; Safat *et al.* 2015). However, GAT1-knockout mice with excessive extracellular GABA displayed mild anxiety and depression-like behaviors (Chiu *et al.* 2005), indicating the side effects of GAT1 overinhibition. GAT3 is almost exclusively expressed by astrocytes (Gadea and López-Colomé 2001). In helpless rats, a validated animal model of depression, reduced expression of GAT3 was found in several brain regions (Zink *et al.* 2009). As the GABA concentration in the synaptic cleft is also regulated by glial cell uptake, increased GAT3 subsequently results in increased GABA uptake. Here, the OVX rats had higher levels of GAT3 in the AMY (119.0%) and higher GAT1 levels in the HYP (Fig. 6a), suggesting decreased GABA levels at the synaptic cleft and a dysregulation of the GABAergic system both in the AMY and HYP. The GABAergic system has been implicated in the pathogenesis of neuropathic pain. During paclitaxel-induced neuropathic pain, there is a significant increase in GAT1 in the anterior cingulate cortex (ACC) (Masocha 2015). In rats with paclitaxel-induced neuropathic pain, the protein expression of GAT1 was increased, while GAT3 was decreased in the spinal dorsal horn (Yadav *et al.* 2015). Pharmacological inhibition of GAT1 ameliorates the paclitaxel-induced suppression of GABAergic tonic inhibition and neuropathic pain (Yadav *et al.* 2015).

Abnormalities of glutamatergic transmission are involved in the pathophysiology of anxiety. In particular, anxiety disorders are regarded as the result of disrupted balance between inhibition and excitation in the brain (Linden *et al.* 2006; Wieronska and Pilc 2009). Group II receptors (mGluR2/3) are primarily localized presynaptically in such diverse brain areas as the cortex, thalamus, striatum, amygdala and hippocampus (Ohishi *et al.* 1994) and are thought to play a critical role in anxiety (Linden *et al.* 2004; Swanson *et al.* 2005; Chiechio and Nicoletti 2012). Group II mGluR antagonists have been demonstrated to improve cognitive behaviors and to alleviate depression and anxiety behaviors in animals (Campo *et al.* 2011; Yoshimizu *et al.* 2006; Kim *et al.* 2014; Pitsikas 2014). Fyn-deficient mice showed heightened anxiety-like behaviors (Miyakawa *et al.* 1996). Here, we found clearly increased levels of mGluR3 in the HIP (107.4%) and decreased levels of Fyn in the AMY (74.4%) of the OVX rats.

The growing concern with estrogen deficiency is the increased incidence of cognitive decline and neurodegenerative diseases, such as AD. The lesions in AD brains include the formation of intracellular neurofibrillary tangles (NFTs) and extracellular senile plaques (SPs), loss of neurons, and impairment of synapses. The defining components of SPs are extracellular collections of aggregated A β , whereas NFTs consist of intracellular hyperphosphorylated tau

(Duyckaerts *et al.* 2009; Fagan *et al.* 2011). The microtubule-associated protein tau plays an important role in stabilizing microtubules, and its hyperphosphorylation promotes microtubule depolymerization. Hyperphosphorylated tau is the major component of NFTs. A recent finding implicated tau as an essential mediator of the adverse effects of stress on brain structure and function (Lopes *et al.* 2016). Here, we found that the OVX rats had hyperphosphorylated tau at the Ser396, Ser404 and Ser198/199/202 sites in the HIP and AMY, which might be a result of the activation of GSK3 β and Phk. Together with hyperphosphorylated tau, decreased HSPA1A levels, which were reported to directly inhibit tau aggregation (Patterson *et al.* 2011), might contribute to the increase of total tau levels in the HYP and AMY of OVX rats.

A β is the product of cleavage of amyloid precursor protein (APP) by β -site APP-cleaving enzyme (BACE1) and γ -secretase. Estrogen decreases A β while upregulating A β -degrading enzymes and multiple studies indicate that loss of ovarian hormones can lead to increased generation or decreased clearance of A β in the brain (Carroll and Pike 2008; Carroll *et al.* 2007; Jaffe *et al.* 1994; Petanceska *et al.* 2000; Zhao *et al.* 2010). In guinea pigs, it was found that OVX increased A β in the brain (Petanceska *et al.* 2000). In the brains of triple-transgenic AD mice, OVX significantly exacerbated mitochondrial dysfunction and increased mitochondrial A β load (Yao *et al.* 2012). However, in the nontransgenic female mouse brain after OVX, researchers only observed mitochondrial dysfunction and oxidative stress (Yao *et al.* 2012). It was reported in ICR mice that OVX did not affect hippocampal A β 40 levels; although it significantly increased serum, A β 40 levels (Fukuzaki *et al.* 2008). In this research, alterations of A β generation or clearance-related proteins varied in different brain regions. γ -secretase is reported to be associated with Erlin-2, and siRNA-mediated knockdown of Erlin-2 resulted in a decrease in A β production (Teranishi *et al.* 2012). In this study, increased Erlin-2 in the HIP and decreased Erlin-2 in the PFC of the OVX rats were shown. SEPT8, which was found to reduce soluble APP β and A β levels in neuronal cells by decreasing levels of BACE1 protein (Kurkinen *et al.* 2016), was increased in the HIP and decreased in the PFC and AMY of the OVX rats. Fbxo2, which facilitates the degradation of BACE1 (Atkin *et al.* 2014), was shown to be increased in the HIP. Interestingly, TTR, which binds to A β to inhibit its aggregation and neurotoxicity and acts as an A β cleavage protein (Silva *et al.* 2017), was shown to be clearly increased in the HIP, HYP and AMY of the OVX rats. All these data indicated that the PFC and AMY might bear A β overproduction earlier than the HIP. In AD processing, A β deposits were first found exclusively in the neocortex in Phase I, then in the allocortical brain regions in Phase II, in the diencephalic nuclei, the striatum, and the cholinergic nuclei of the basal forebrain in Phase III, in several brainstem nuclei in Phase IV, and finally in the cerebellum in Phase V (Thal *et al.* 2002).

Moreover, in most cases of AD (particularly in older AD patients), typical pathological features are accompanied by comorbid lesions, such as vascular abnormalities and aggregates of some non-AD-specific pathogenic proteins such as α -synuclein, β -synuclein, and γ -synuclein (Knopman *et al.* 2003; Oeckl *et al.* 2016). In this study, dysfunction of the endothelial barrier in the brain after OVX was suggested by decreased levels of MYADM in the HIP and HYP and decreased levels of Cavin-1 in the AMY. MYADM controls endothelial barrier function (Aranda *et al.* 2013), and deficiency of Cavin-1 induced dysfunction of the small arteries (Sward *et al.* 2014). Additionally, increased γ -synuclein in the HYP (129.5%) and AMY (131.2%) were shown (Fig. 3c).

In the brain, estrogen acts through its receptors, ER α and ER β . The HIP is one of the most important brain regions involved in cognition, and the level of hippocampal ER α is decreased in some neurological diseases that influence cognition including AD (Ishunina *et al.* 2007) and mood disorder (Perlman *et al.* 2005), while ER β may increase in AD patients (Savaskan *et al.* 2001). Previous research in rats also showed that long-term ovariectomy led to a significant decrease in hippocampal ER α but not ER β (Qu *et al.* 2013; Zhang *et al.* 2011). Our previous studies noted that ER α rescue is effective in improving the hippocampal-dependent cognition deficit after long-term ovariectomy (Qu *et al.* 2013; Qu *et al.* 2016). Estrogens and their receptors in the medial AMY rapidly facilitate social recognition in female mice (Lymer *et al.* 2018). A recent study in the AMY of the guinea pig reported that in various nuclei of the AMY, small subsets of CB neurons and substantial proportions of PV neurons coexpress ER β , while many of the CR neurons coexpress ER α . Both of these estrogen-sensitive populations are strictly separated, as CB and PV neurons almost never coexpress ER α , while CR cells are usually devoid of ER β (Równiak 2017). By Western blotting, we observed that ER α and ER β both were decreased in the AMY of the OVX rats. The role of ER β in emotional behaviors including depression, anxiety, and aggression has been proved by several studies in ER $\beta^{-/-}$ mice (Rocha *et al.* 2005; Imwalle *et al.* 2005), and GABA inhibition is suggested to be involved in the neuroprotection of ER β in these abnormal emotional behaviors (Murphy *et al.* 1998; Herbison 1997). ER β localizes extensively with parvalbumin-labeled inhibitory neurons in the cortex, amygdala, basal forebrain, and hippocampal formation of intact and ovariectomized adult rats (Blurton-Jones and Tuszynski 2002). Therefore, further studies are required to verify the cell types bearing increased CR in the AMY and increased PV in the PFC and HIP of OVX rats.

Conclusions

In this research, we reproduced a surgical menopause rat model with estrogen deprivation induced by bilateral OVX, which showed depressive and dementia-related behaviors in the OVX rats. The numbers of microglia in the HIP and AMY and the numbers of astrocytes in the PFC, HYP and AMY were significantly increased after OVX, while neuronal loss was

This article is protected by copyright. All rights reserved.

shown in the PFC, HIP, HYP and AMY. By mass spectrometric analysis and Western blotting, it was shown that ER stress and mitochondrial dysfunction triggered apoptosis involved in OVX-induced neuronal loss. Synaptic impairments, cytoskeletal abnormalities, injury of myelin and dysfunction of oligodendrocytes were also observed in the OVX rats. The observed dysregulation of excitatory and inhibitory neurotransmissions in the AMY might be responsible for the OVX-induced depressive behaviors. Collectively, our study showed the changes related to depression and dementia in different brain regions after OVX, which is beneficial for understanding the pathophysiologic mechanism in menopause related to brain injuries and for searching for potential targets for early intervention.

--Human subjects --

Involves human subjects:

If yes: Informed consent & ethics approval achieved:

=> if yes, please ensure that the info "Informed consent was achieved for all subjects, and the experiments were approved by the local ethics committee." is included in the Methods.

ARRIVE guidelines have been followed:

Yes

=> if No or if it is a Review or Editorial, skip complete sentence => if Yes, insert "All experiments were conducted in compliance with the ARRIVE guidelines." unless it is a Review or Editorial

Acknowledgements

This work was supported by grants from the Natural Science Foundation of China (91539112) and Integrated Innovative Team for Major Human Diseases Program of Tongji Medical College. We thank Jingjie PTM BioLab Co. Ltd. (Hangzhou, China) for the mass spectrometry analysis.

This article is protected by copyright. All rights reserved.

Conflict of interest

The authors declare no conflicts of interest.

References

- Almey, A., Milner, T. A., Brake, W. G. (2015) Estrogen receptors in the central nervous system and their implication for dopamine-dependent cognition in females. *Horm. Behav.* **74**, 125–138.
- Andrews, B., Carroll, J., Ding, S., Fearnley, I. M., Walker, J.E. (2013) Assembly factors for the membrane arm of human complex I. *Proc. Natl. Acad. Sci. U. S. A.* **110**, 18934–18939.
- Aranda, J.F., Reglero-Real, N., Marcos-Ramiro, B., Ruiz-Sáenz, A., Fernández-Martín, L., Bernabé-Rubio, M., Kremer, L., *et al.* (2013) MYADM controls endothelial barrier function through ERM-dependent regulation of ICAM-1 expression. *Mol. Biol. Cell* **24**, 483–494.
- Asante, D., Stevenson, N.L., Stephens, D.J. (2014) Subunit composition of the human cytoplasmic dynein-2 complex. *J. Cell Sci.* **127**, 4774–4787.
- Atkin, G., Hunt, J., Minakawa, E., Sharkey, L., Tipper, N., Tennant, W., Paulson, H.L. (2014) F-box only protein 2 (Fbxo2) regulates amyloid precursor protein levels and processing. *J. Biol. Chem.* **289**, 7038–7048.
- Atkin, G., Moore, S., Lu, Y., Nelson, R. F., Tipper, N., Rajpal, G., Hunt, J., *et al.* (2015) Loss of F-box Only Protein 2 (Fbxo2) Disrupts Levels and Localization of Select NMDA Receptor Subunits, and Promotes Aberrant Synaptic Connectivity. *J. Neurosci.* **35**, 6165–6178.
- Atwood C. S., Bowen, R. L. (2015) The endocrine dyscrasia that accompanies menopause and andropause induces aberrant cell cycle signaling that triggers re-entry of post-mitotic neurons into the cell cycle, neurodysfunction, neurodegeneration and cognitive disease. *Horm Behav.* **76**:63-80.
- Azoulay-Zohar H., Israelson A., Abu-Hamad S., Shoshan-Barmatz V. (2004) In self-defence: hexokinase promotes voltage-dependent anion channel closure and prevents mitochondria-mediated apoptotic cell death. *Biochem. J.* **377**, 347–355.
- Barth, C., Villringer, A., Sacher, J. (2015) Sex hormones affect neurotransmitters and shape the adult female brain during hormonal transition periods. *Front. Neurosci.* **9**, 37.
- Bastos, C.P., Pereira, L.M., Ferreira-Vieira, T.H., Drumond, L.E., Massensini, A.R., Moraes, M.F.D., Pereira, G.S. (2015) Object recognition memory deficit and depressive-like behavior caused by

This article is protected by copyright. All rights reserved.

chronic ovariectomy can be transitorially recovered by the acute activation of hippocampal estrogen receptors. *Psychoneuroendocrinology* **57**, 14–25.

- Bean, L. A., Ianov, L., Foster, T. C. (2014) Estrogen Receptors, the Hippocampus, and Memory. *Neuroscientist* **20**, 534–545.
- Berna-Erro, A., Jardin, I., Salido, G. M., Rosado, J. A. (2017) Role of STIM2 in cell function and physiopathology. *J. Physiol.* **595**, 3111–3128.
- Blurton-Jones, M., Tuszynski, M.H. (2002) Estrogen receptor-beta colocalizes extensively with parvalbumin-labeled inhibitory neurons in the cortex, amygdala, basal forebrain, and hippocampal formation of intact and ovariectomized adult rats. *J. Comp. Neurol.* **452**, 276–287.
- Braunewell, K. H. (2012) The visinin-like proteins VILIP-1 and VILIP-3 in Alzheimer’s disease—old wine in new bottles. *Front. Mol. Neurosci.* **5**, 20.
- Brinton, R. D., Yao, J., Yin, F., Mack, W. J., Cadenas, E. (2015) Perimenopause as a neurological transition state. *Nat. Rev. Endocrinol.* **11**: 393–405.
- Buffalari D. M., See R. E. (2010) Amygdala mechanisms of Pavlovian psychostimulant conditioning and relapse. *Curr. Top. Behav. Neurosci.* **3**, 73-99.
- Cahill, L. (2006) Why sex matters for neuroscience. *Nat. Rev. Neurosci.* **7**, 477–484.
- Campbell S, Whitehead M. (1977) Oestrogen therapy and the menopausal syndrome. *Clin Obstet Gynaecol.* **4**, 31-47.
- Campo, B., Kalinichev, M., Lambeng, N., El Yacoubi, M., Royer-Urios, I., Schneider, M., Legrand, C., Parron, D., et al. (2011) Characterization of an mGluR2/3 negative allosteric modulator in rodent models of depression. *J Neurogenet.* **25**: 152–66.
- Carroll J. C., Pike C. J. (2008) Selective estrogen receptor modulators differentially regulate Alzheimer-like changes in female 3xTg-AD mice. *Endocrinology* **149**, 2607–2611.
- Carroll J. C., Rosario E. R., Chang L., Stanczyk F. Z., Oddo S., LaFerla F. M., Pike C. J. (2007) Progesterone and Estrogen Regulate Alzheimer-Like Neuropathology in Female 3xTg-AD Mice. *J. Neurosci.* **27**, 13357–13365.
- Cartmell, J., Monn, J. A., Schoepp, D. D. (1999) The metabotropic glutamate 2/3 receptor agonists LY354740 and LY379268 selectively attenuate phencyclidine versus d-amphetamine motor behaviors in rats. *J. Pharmacol. Exp. Ther.* **291**, 161–170.
- Chiechio, S. (2016) Modulation of Chronic Pain by Metabotropic Glutamate Receptors. *Adv. Pharmacol.* **75**, 63–89.

Chiechio, S., Nicoletti, F. (2012) Metabotropic glutamate receptors and the control of chronic pain. *Curr Opin Pharmacol.* **12**: 28–34.

Chiu, C. S., Brickley, S., Jensen, K., Southwell, A., Mckinney, S., Cull-Candy, S., Mody, I., Lester, H. A. (2005) GABA transporter deficiency causes tremor, ataxia, nervousness, and increased GABA-induced tonic conductance in cerebellum. *J Neurosci.* **25** :3234–3245.

Choudhury, K.R., Bucha, S., Baksi, S., Mukhopadhyay, D., Bhattacharyya, N.P. (2016) Chaperone-like protein HYPK and its interacting partners augment autophagy. *Eur. J. Cell Biol.* **95**, 182–194.

Corbetta S., Gualdoni S., Ciceri G., Monari M., Zuccaro E., Tybulewicz V. L. J., Curtis I. de (2009) Essential role of Rac1 and Rac3 GTPases in neuronal development. *FASEB J.* **23**, 1347–1357.

Dalal, P. K., Agarwal, M. (2015) Postmenopausal syndrome. *Indian J Psychiatry.* **57**(Suppl 2): S222–S232.

Dou, H., Birusingh, K., Faraci, J., Gorantla, S., Poluektova, L.Y., Maggirwar, S.B., Dewhurst, S., *et al.* (2003) Neuroprotective activities of sodium valproate in a murine model of human immunodeficiency virus-1 encephalitis. *J. Neurosci.* **23**, 9162–9170.

Duyckaerts C., Panchal M., Delatour B., Potier M.C. (2009) [Morphologic and molecular neuropathology of Alzheimer's disease]. *Ann. Pharm. Fr.* **67**, 127–135.

Estrada, C. M., Ghisays, V., Nguyen, E. T., Caldwell, J. L., Streicher, J., Solomon, M. B. (2018) Estrogen signaling in the medial amygdala decreases emotional stress responses and obesity in ovariectomized rats. *Horm. Behav.* **98**, 33–44.

Fagan, A.M., Shaw, L.M., Trojanowski, J.Q., Morris, J.C., Holtzman, D.M. (2011) Comparison of analytical platforms for cerebrospinal fluid measures of A β 1-42, total tau and p-tau181 for identifying Alzheimer's disease amyloid plaque pathology. *Arch. Neurol.* **68**, 1137–1144.

Fowler, S.L., Akins, M., Zhou, H., Figeys, D., Bennett, S.A.L. (2013) The liver connexin32 interactome is a novel plasma membrane-mitochondrial signaling nexus. *J. Proteome Res.* **12**, 2597–2610.

Fukuzaki E., Takuma K., Funatsu Y., Himeno Y., Kitahara Y., Gu B., Mizoguchi H., *et al.* (2008) Ovariectomy increases neuronal amyloid-beta binding alcohol dehydrogenase level in the mouse hippocampus. *Neurochem Int.* **52**, 1358-1364.

Gadea, A., López-Colomé, A. M. (2001) Glial transporters for glutamate, glycine, and GABA: II. GABA transporters. *J Neurosci Res.* **63**: 461–468.

- Gordon, J.L., Rubinow, D.R., Eisenlohr-Moul, T.A., Xia, K., Schmidt, P.J., Girdler, S.S. (2018) Efficacy of Transdermal Estradiol and Micronized Progesterone in the Prevention of Depressive Symptoms in the Menopause Transition. *JAMA Psychiatry* **3366**, 1–9.
- Herbison, A.E. (1997) Estrogen regulation of GABA transmission in rat preoptic area. *Brain Res. Bull.* **44**, 321–326.
- Imwalle, D.B., Gustafsson, J.Å., Rissman, E.F. (2005) Lack of functional estrogen receptor β influences anxiety behavior and serotonin content in female mice. *Physiol. Behav.* **84**, 157–163.
- Ishunina, T.A., Fischer, D.F., Swaab, D.F., 2007. Estrogen receptor α and its splice variants in the hippocampus in aging and Alzheimer's disease. *Neurobiol. Aging* **28**, 1670–1681.
- Ito, H., Atsuzawa, K., Morishita, R., Usuda, N., Sudo, K., Iwamoto, I., Mizutani, K., *et al.* (2009) Sept8 controls the binding of vesicle-associated membrane protein 2 to synaptophysin. *J. Neurochem.* **108**, 867–880.
- Jacome L.F., Gautreaux C., Inagaki T., Mohan G., Alves S., Lubbers L.S., Luine V. (2010) Estradiol and ERbeta agonists enhance recognition memory, and DPN, an ERbeta agonist, alters brain monoamines. *Neurobiol. Learn. Mem.* **94**, 488–498.
- Jaffe A. B., Toran-Allerand C. D., Greengard P., Gandy S. E. (1994) Estrogen regulates metabolism of Alzheimer amyloid β precursor protein. *J. Biol. Chem.* **269**, 13065–13068.
- Jain, S., Yoon, S.Y., Zhu, L., Brodbeck, J., Dai, J., Walker, D., Huang, Y. (2012) Arf4 Determines Dentate Gyrus-Mediated Pattern Separation by Regulating Dendritic Spine Development. *PLoS One* **7**, e46340.
- Jiang, T.T., Wang, C., Wei, L.L., Yu, X.M., Shi, L.Y., Xu, D.D., Chen, Z.L., *et al.* (2015) Serum protein gamma-glutamyl hydrolase, Ig gamma-3 chain C region, and haptoglobin are associated with the syndromes of pulmonary tuberculosis in traditional Chinese medicine. *BMC Complement. Altern. Med.* **15**, 243.
- Kantarci, K., Tosakulwong, N., Lesnick, T. G., Zuk, S. M., Lowe, V. J., Fields, J. A., Gunter, J. L. *et al.* (2018) Brain structure and cognition 3 years after the end of an early menopausal hormone therapy trial. *Neurology.* **90** :e1404–e1412.
- Kim, S. H., Steele, J. W., Lee, S. W., Clemenson, G. D., Carter, T. A., Treuner, K., Gadiant, R., Wedel, P., *et al.* (2014) Proneurogenic Group II mGluR antagonist improves learning and reduces anxiety in Alzheimer A β oligomer mouse. *Mol Psychiatry.* **19**: 1235–1242.

- Knopman, D. S., Parisi, J. E., Boeve, B. F., Cha, R. H., Apaydin H., Salviati, A., Edland S. D., Rocca W. A. (2003) Vascular dementia in a population-based autopsy study. *Arch. Neurol.* **60**, 569–575.
- Kodaman, P.H.M.D.P.D. (2010) Early Menopause: Primary Ovarian Insufficiency and Surgical Menopause. *Semin. Reprod. Med.* **28**, 360–369.
- Kuiper, G. G. J. M., Shughrue, P. J., Merchenthaler, I., Gustafsson, J. Å. (1998) The estrogen receptor β subtype: A novel mediator of estrogen action in neuroendocrine systems. *Front. Neuroendocrinol.* **19**, 253–286.
- Kurkinen, K. M. A., Martinen, M., Turner, L., Natunen, T., Mäkinen, P., Haapalinna, F., Sarajärvi, T., *et al.* (2016) SEPT8 modulates β -amyloidogenic processing of APP by affecting the sorting and accumulation of BACE1. *J. Cell Sci.* **129**, 2224–2238.
- LeDoux J. E. (1993) Emotional memory systems in the brain. *Behav. Brain. Res.* **58**, 69-79.
- Linden, A. M., Baez, M., Bergeron, M., Schoepp, D. D. (2006) Effects of mGlu2 or mGlu3 receptor deletions on mGlu2/3 receptor agonist (LY354740)-induced brain c-Fos expression: specific roles for mGlu2 in the amygdala and subcortical nuclei, and mGlu3 in the hippocampus. *Neuropharmacology.* **51**: 213–528.
- Linden, A. M., Greene, S. J., Bergeron, M., Schoepp, D. D. (2004) Anxiolytic activity of the MGLU2/3 receptor agonist LY354740 on the elevated plus maze is associated with the suppression of stress-induced c-Fos in the hippocampus and increases in c-Fos induction in several other stress-sensitive brain regions. *Neuropsychopharmacology.* **29**: 502–513.
- Lopes, S., Vaz-Silva, J., Pinto, V., Dalla, C., Kokras, N., Bedenk, B., Mack, N., *et al.* (2016) Tau protein is essential for stress-induced brain pathology. *Proc. Natl. Acad. Sci.* **113**, E3755–E3763.
- Lymer, J.M., Sheppard, P.A.S., Kuun, T., Blackman, A., Jani, N., Mahbub, S., Choleris, E. (2018) Estrogens and their receptors in the medial amygdala rapidly facilitate social recognition in female mice. *Psychoneuroendocrinology* **89**, 30–38.
- Maekawa, S., Kobayashi, Y., Odagaki, S.I., Makino, M., Kumanogoh, H., Nakamura, S., Morita, M., Hayashi, F. (2013) Interaction of NAP-22 with brain glutamic acid decarboxylase (GAD). *Neurosci. Lett.* **537**, 50–54.
- Maki, P. M. (2013) Critical window hypothesis of hormone therapy and cognition: A scientific update on clinical studies. *Menopause.* **20**, 695–709.

- Marsh, W. K., Bromberger, J. T., Crawford, S. L., Leung, K., Kravitz, H. M., Randolph, J. F., Joffe, H., Soares, C. N. (2017) Lifelong estradiol exposure and risk of depressive symptoms during the transition to menopause and postmenopause. *Menopause* **24**, 1351–1359.
- Masocha, W. (2015) Comprehensive analysis of the GABAergic system gene expression profile in the anterior cingulate cortex of mice with Paclitaxel-induced neuropathic pain. *Gene. Expr.* **16**, 145–153.
- Mielke M. M., Vemuri P., Rocca W. A. (2014) Clinical epidemiology of Alzheimer's disease: assessing sex and gender differences. *Clin. Epidemiol.* **6**:37–48.
- Miyakawa, T., Yagi, T., Kagiya, A., Niki, H. (1996) Radial maze performance, open-field and elevated plus-maze behaviors in Fyn-kinase deficient mice: further evidence for increased fearfulness. *Brain. Res. Mol. Brain. Res.* **37**, 145–150.
- Monteiro, P., Feng, G. (2017) SHANK proteins: Roles at the synapse and in autism spectrum disorder. *Nat. Rev. Neurosci.* **18**, 147–157.
- Muller J. F., Mascagni F., McDonald A. J. (2007) Postsynaptic targets of somatostatin -containing interneurons in the rat basolateral amygdala. *J Comp Neurol* **500**, 513–529.
- Murphy, D. D., Cole, N. B., Greenberger, V., Segal, M. (1998) Estradiol increases dendritic spine density by reducing GABA neurotransmission in hippocampal neurons. *J. Neurosci.* **18**, 2550–2559.
- Ning, L. -N., Zhang, T., Chu, J., Qu, N., Lin, L., Fang, Y. -Y., Shi, Y., et al. (2018) Gender-Related Hippocampal Proteomics Study from Young Rats After Chronic Unpredicted Mild Stress Exposure. *Mol. Neurobiol.* **55**, 835–850.
- Nygaard, H. B. (2018) Targeting Fyn Kinase in Alzheimer's Disease. *Biol. Psychiatry* **83**, 369–376.
- O'Bryant, S. E., Palay, A., McCaffrey, R. J. (2003) A Review of Symptoms Commonly Associated with Menopause: Implications for Clinical Neuropsychologists and Other Health Care Providers. *Neuropsychol. Rev.* **13**, 145–152.
- Oeckl, P., Metzger, F., Nagl, M., von Arnim, C. A. F., Halbgebauer, S., Steinacker, P., Ludolph, A.C., Otto, M. (2016) Alpha-, Beta-, and Gamma-synuclein Quantification in Cerebrospinal Fluid by Multiple Reaction Monitoring Reveals Increased Concentrations in Alzheimer's and Creutzfeldt-Jakob Disease but No Alteration in Synucleinopathies. *Mol. Cell. Proteomics* **15**, 3126–3138.

- Ohishi, H., Ogawa-Meguro, R., Shigemoto, R., Kaneko, T., Nakanishi, S., Mizuno, N. (1994) Immunohistochemical localization of metabotropic glutamate receptors, mGluR2 and mGluR3, in rat cerebellar cortex. *Neuron*. **13**: 55–66.
- Öhrfelt, A., Johansson, P., Wallin, A., Andreasson, U., Zetterberg, H., Blennow, K., Svensson, J. (2016) Increased Cerebrospinal Fluid Levels of Ubiquitin Carboxyl-Terminal Hydrolase L1 in Patients with Alzheimer's Disease. *Dement. Geriatr. Cogn. Dis. Extra* **6**, 283–294.
- Patterson, K. R., Ward, S. M., Combs, B., Voss, K., Nicholas, M., Morfini, G., Brady, S. T., Gamblin, T. C., Binder, L. I. (2011) Heat shock protein 70 prevents both tau aggregation and the inhibitory effects of preexisting tau aggregates on fast axonal transport. *Biochemistry* **50**, 10300–10310.
- Peng, X., Wang, L., Chen, G., Wang, X. (2012) Dynamic expression of adenylate kinase 2 in the hippocampus of pilocarpine model rats. *J. Mol. Neurosci.* **47**, 150–157.
- Perlman, W. R., Tomaskovic-Crook, E., Montague, D. M., Webster, M. J., Rubinow, D. R., Kleinman, J. E., Weickert, C. S. (2005) Alteration in estrogen receptor α mRNA levels in frontal cortex and hippocampus of patients with major mental illness. *Biol. Psychiatry* **58**, 812–824.
- Petanceska S. S., Nagy V., Frail D., Gandy S. (2000) Ovariectomy and 17 β -estradiol modulate the levels of Alzheimer's amyloid beta peptides in brain. *Exp. Gerontol.* **35**, 1317–1325.
- Pitsikas, N. (2014) The metabotropic glutamate receptors: potential drug targets for the treatment of anxiety disorders? *Eur J Pharmacol.* **723**: 181–184.
- Polletta, L., Vernucci, E., Carnevale, I., Arcangeli, T., Rotili, D., Palmerio, S., Steegborn, C., *et al.* (2015) SIRT5 regulation of ammonia-induced autophagy and mitophagy. *Autophagy* **11**, 253–270.
- Qu, N., Wang, L., Liu, Z. C., Tian, Q., Zhang, Q. (2013) Oestrogen receptor α agonist improved long-term ovariectomy-induced spatial cognition deficit in young rats. *Int. J. Neuropsychopharmacol.* **16**, 1071–1082.
- Qu, N., Zhou, X. Y., Han, L., Wang, L., Xu, J. X., Zhang, T., Chu, J., *et al.* (2016) Combination of PPT with LiCl Treatment Prevented Bilateral Ovariectomy -Induced Hippocampal-Dependent Cognition Deficit in Rats. *Mol. Neurobiol.* **53**, 894–904.
- Rocha, B. A., Fleischer, R., Schaeffer, J. M., Rohrer, S. P., Hickey, G. J. (2005) 17 β -Estradiol -induced antidepressant-like effect in the Forced Swim Test is absent in estrogen receptor- β knockout (BERKO) mice. *Psychopharmacology (Berl)*. **179**, 637–643.

- Równiak, M. (2017) The neurons expressing calcium-binding proteins in the amygdala of the guinea pig: precisely designed interface for sex hormones. *Brain Struct. Funct.* **222**, 3775–3793.
- Sah, P., Faber, E. S. L., Lopez De Armentia, M., Power, J. (2003) The amygdaloid complex: anatomy and physiology. *Physiol Rev* **83**, 803–834.
- Salat, K., Podkowa, A., Kowalczyk, P., Kulig, K., Dziubina, A., Filipek, B., Librowski, T. (2015) Anticonvulsant active inhibitor of GABA transporter subtype 1, tiagabine, with activity in mouse models of anxiety, pain and depression. *Pharmacol. Rep.* **67**, 465–672.
- Sarrel P. M., Sullivan S. D., Nelson L. M. (2016) Hormone replacement therapy in young women with surgical primary ovarian insufficiency. *Fertil Steril.* **106**, 1580–1587.
- Savaskan, E., Olivieri, G., Meier, F., Ravid, R., Muller-spahn, F. (2001) Hippocampal estrogen b-receptor immunoreactivity is increased in Alzheimer's disease. *Brain Res.* **908**, 113–119.
- Shao, Y., Li, X., Lu, Y., Liu, L., Zhao, P. (2015) Aberrant LRP16 protein expression in primary neuroendocrine lung tumors. *Int. J. Clin. Exp. Pathol.* **8**, 6560–6565.
- Sharma, K., Schmitt, S., Bergner, C. G., Tyanova, S., Kannaiyan, N., Manrique-Hoyos, N., Kongi, K., et al. (2015) Cell type- and brain region-resolved mouse brain proteome. *Nat. Neurosci.* **18**, 1819–1831.
- Sherwin BB. (1998) Estrogen and cognitive functioning in women. *Proc Soc Exp Biol Med.* **217**, 17–22.
- Shinoda, Y., Ishii, C., Fukazawa, Y., Sadakata, T., Ishii, Y., Sano, Y., Iwasato, T., et al. (2016) CAPS1 stabilizes the state of readily releasable synaptic vesicles to fusion competence at CA3-CA1 synapses in adult hippocampus. *Sci. Rep.* **6**, 31540.
- Shughrue, P.J., Merchenthaler, I. (2001) Distribution of estrogen receptor beta immunoreactivity in the rat central nervous system. *J. Comp. Neurol.* **436**, 64–81.
- Silva, C. S., Eira, J., Ribeiro, C. A., Oliveira, Â., Sousa, M. M., Cardoso, I., Liz, M. A. (2017) Transthyretin neuroprotection in Alzheimer's disease is dependent on proteolysis. *Neurobiol. Aging* **59**, 10–14.
- Sironi, J. J., Yen, S. H., Gondal, J. A., Wu, Q., Grundke-Iqbal, I., Iqbal, K. (1998) Ser-262 in human recombinant tau protein is a markedly more favorable site for phosphorylation by CaMKII than PKA or PhK. *FEBS Lett.* **436**, 471–475.
- Sorvari, H., Soininen, H., Pitkanen, A. (1996) Caretinin-immunoreactive cells and fibers in the human amygdaloid complex. *J Comp Neurol* **369**, 188–208.

- Spencer J. L., Waters E. M., Romeo R. D., Wood G. E., Milner T. A., McEwen B. S. (2008) Uncovering the mechanisms of estrogen effects on hippocampal function. *Front. Neuroendocrinol.* **29**, 219–237.
- Su, J., Sripanidkulchai K., Hu Y., Wyss J. M., Sripanidkulchai B. (2012) The effect of ovariectomy on learning and memory and relationship to changes in brain volume and neuronal density. *Int. J. Neurosci.* **122**, 549–559.
- Sun, M. K., Alkon, D. L. (2012) Activation of Protein Kinase C Isozymes for the Treatment of Dementias. *Adv. Pharmacol.* **64**, 273–302.
- Swanson, C. J., Bures, M., Johnson, M. P., Linden, A. M., Monn, J. A., Schoepp, D. D. (2005) Metabotropic glutamate receptors as novel targets for anxiety and stress disorders. *Nat Rev Drug Discov.* **4**: 131–144.
- Swärd, K., Albinsson, S., Rippe, C. (2014) Arterial dysfunction but maintained systemic blood pressure in cavin-1-deficient mice. *PLoS One.* **9**, e92428.
- Teranishi, Y., Hur, J. Y., Gu, G. J., Kihara, T., Ishikawa, T., Nishimura, T., Winblad, B., *et al.* (2012) Erlin-2 is associated with active γ -secretase in brain and affects amyloid β -peptide production. *Biochem. Biophys. Res. Commun.* **424**, 476–481.
- Thal, D. R., Rub, U., Orantes, M., Braak, H. (2002) Phases of A beta-deposition in the human brain and its relevance for the development of AD. *Neurology* **58**, 1791–1800.
- Thoeringer, C. K., Erhardt, A., Sillaber, I., Mueller, M. B., Ohl, F., Holsboer, F., Keck, M. E. (2010) Long-term anxiolytic and antidepressant-like behavioural effects of tiagabine, a selective GABA transporter-1 (GAT-1) inhibitor, coincide with a decrease in HPA system activity in C57BL/6 mice. *J Psychopharmacol.* **24**: 733–43.
- Wallace M., Luine V., Arellanos A., Frankfurt M. (2006) Ovariectomized rats show decreased recognition memory and spine density in the hippocampus and prefrontal cortex. *Brain Res.* **1126**, 176–182.
- Wang, K. K., Yang, Z., Sarkis, G., Torres, I., Raghavan, V. (2017) Ubiquitin C-terminal hydrolase-L1 (UCH-L1) as a therapeutic and diagnostic target in neurodegeneration, neurotrauma and neuro-injuries. *Expert Opin. Ther. Targets* **21**, 627–638.
- Whitmer R. A., Quesenberry C. P., Zhou, J., Yaffe, K. (2011) Timing of hormone therapy and dementia: the critical window theory revisited. *Ann. Neurol.* **69**, 163–169.
- Wierońska, J. M., Pilc, A. (2009) Metabotropic glutamate receptors in the tripartite synapse as a target for new psychotropic drugs. *Neurochem Int.* **55**: 85–97.

- Accepted Article
- Wijdeven, R. H., Janssen, H., Nahidiazar, L., Janssen, L., Jalink, K., Berlin, I., Neefjes, J. (2016) Cholesterol and ORP1L-mediated ER contact sites control autophagosome transport and fusion with the endocytic pathway. *Nat. Commun.* **7**, 11808.
- Woodruff, A. R., Sah, P. (2007) Networks of Parvalbumin-Positive Interneurons in the Basolateral Amygdala. *J. Neurosci.* **27**, 553–563.
- Xu X., Gu, T., Shen Q. (2015) Different effects of bisphenol-A on memory behavior and synaptic modification in intact and estrogen-deprived female mice. *J. Neurochem.* **132**, 572–582.
- Yadav, R., Yan, X., Maixner, D. W., Gao, M., Weng, H. R. (2015) Blocking the GABA transporter GAT-1 ameliorates spinal GABAergic disinhibition and neuropathic pain induced by paclitaxel. *J. Neurochem.* **133**, 857–869.
- Yang, Y., Qin, M., Bao, P., Xu, W., Xu, J. (2017) Secretory carrier membrane protein 5 is an autophagy inhibitor that promotes the secretion of α -synuclein via exosome. *PLoS One* **12**, e180892.
- Yao J., Irwin R., Chen S., Hamilton R., Cadenas E., Brinton R. D. (2012) Ovarian hormone loss induces bioenergetic deficits and mitochondrial β -amyloid. *Neurobiol. Aging* **33**, 1507–1521.
- Yoshimizu, T., Shimazaki, T., Ito, A., Chaki, S. (2006) An mGluR2/3 antagonist, MGS0039, exerts antidepressant and anxiolytic effects in behavioral models in rats. *Psychopharmacology (Berl)*. **186**: 587–93.
- Yun, H. S., Baek, J. H., Yim, J. H., Lee, S. J., Lee, C. W., Song, J. Y., Um, H. D., *et al.* (2014) Knockdown of hepatoma-derived growth factor-related protein-3 induces apoptosis of H1299 cells via ROS-dependent and p53-independent NF- κ B activation. *Biochem. Biophys. Res. Commun.* **449**, 471–476.
- Zhang, Q. -g., Han, D., Wang, R. -m., Dong, Y., Yang, F., Vadlamudi, R. K., Brann, D. W. (2011) C terminus of Hsc70-interacting protein (CHIP)-mediated degradation of hippocampal estrogen receptor-alpha and the critical period hypothesis of estrogen neuroprotection. *Proc. Natl. Acad. Sci.* **108**, E617–E624.
- Zhang, Y., Chen, K., Sloan, S. A., Bennett, M. L., Scholze, A. R., O’Keeffe, S., Phatnani, H. P., *et al.* (2014) An RNA-Sequencing Transcriptome and Splicing Database of Glia, Neurons, and Vascular Cells of the Cerebral Cortex. *J. Neurosci.* **34**, 11929–11947.
- Zhao L., Yao J., Mao Z., Chen S., Wang Y., Brinton R. D. (2011) 17 β -Estradiol regulates insulin-degrading enzyme expression via an ER β /PI3-K pathway in hippocampus: Relevance to Alzheimer’s prevention. *Neurobiol. Aging* **32**, 1949–1963.

Zhao, X. H., Zhao, Y. Q., Zhu, C., Chen, L., Hu, W., Zhang, T., Dong, Y. L., Wu, S. X., Kaye, A. D., Wang, W., Li, Y. Q. (2015) Different analgesic effects of intrathecal endomorphin-2 on thermal hyperalgesia and evoked inflammatory pain in ovariectomized rats. *Pain. Physician.* **18**: 195–205.

Zhou, Y., Takahashi, E., Li, W., Halt, A., Wiltgen, B., Ehninger, D., Li, G. -D., *et al.* (2007) Interactions between the NR2B Receptor and CaMKII Modulate Synaptic Plasticity and Spatial Learning. *J. Neurosci.* **27**, 13843–13853.

Zhu, H., Yan, H., Tang, N., Li, X., Pang, P., Li, H., Chen, W., *et al.* (2017) Impairments of spatial memory in an Alzheimer's disease model via degeneration of hippocampal cholinergic synapses. *Nat. Commun.* **8**, 1676.

Zink, M., Vollmayr, B., Gebicke-Haerter, P. J., Henn, F. A. (2009) Reduced expression of GABA transporter GAT3 in helpless rats, an animal model of depression. *Neurochem Res.* **34**: 1584–1593.

Figure Legends

Figure 1. A time-line diagram for the overall research. Three-month-old female Sprague-Dawley (SD) rats were divided into 2 groups, the sham-operated group (SHAM, n = 18) and ovariectomized group (OVX, n = 18). From the 2nd week to 7th week after surgery, the open field test (OFT) was performed to evaluate locomotor activities of the rats once a week. In the 7th week after operation, the sucrose preference test (SPT) and forced swimming test (FST) were performed. In the 8th week after the operation, the Morris water maze test (MWMT) was performed. Samples were taken rapidly after the MWMT.

Figure 2. OVX rats showed depressive behavior and cognitive impairments.

Three-month-old female SD rats were divided into 2 groups, the SHAM group (n = 18) and OVX group (n = 18). The OFT, SPT, FST, and MWMT were used to evaluate behavioral changes in the rats. The number of rearing responses (a), moving duration (b), the total distance (c) and the number of zone crossings (d) of the rats in the OFT were recorded from the 2nd to 7th week after the operation. In the 7th week, the percentage of sucrose consumption (e) and the immobility time within 5 min in the FST (f) were recorded. In the MWMT in the 8th week after the operation, the latencies to find the platform in the learning period (g), the latencies of the first platform crossing (h) and the mean annulus crossings within 60 s (i) in the memory period were traced. After the MWMT, the plasma levels of 17 β -estradiol were detected by ELISA (j). The levels of ER α and ER β in the hippocampus (HIP) and amygdala (AMY) were detected by Western blotting (k) and quantitative analysis (l, m) (n = 6/group). Data are presented as the means \pm SEM. * $p < 0.05$, ** $p < 0.01$, *** $p < 0.001$, versus SHAM.

Figure 3. Brain damage-related proteins and neuronal loss in the OVX rats. A total of 146 differentially expressed proteins were obtained in this study. Their subcellular classifications (a) and cell properties (b) in the prefrontal cortex (PFC), hippocampus (HIP), hypothalamus (HYP) and amygdala (AMY) are shown. The differentially expressed proteins related to brain damage are listed with a ratio (OVX/SHAM, c), including Ras-related C3 botulinum toxin substrate 1 (Rac1), Rac3, ubiquitin C-terminal hydrolase-L1 (UCH-L1), leukemia-related protein 16 (LRP16), S100A1, stromal interaction molecule 2 (STIM2), γ -synuclein (SNCG), ER lipid raft-associated protein 2 (Erlin-2), hepatoma-derived growth factor-related protein-3 (HRP-3), protein kinase C (PKC) ζ , PKC δ , PKC ϵ , PKC β , transthyretin (TTR), myelin proteolipid protein (PLP), myelin-associated glycoprotein (MAG), myelin basic protein (MBP), neuronal membrane glycoprotein M6-a (GM6A), neuronal membrane glycoprotein M6-b (GM6B), myeloid-associated differentiation marker (MYADM), and polymerase-1 and transcript release factor (PTRF). Red color indicates the increased proteins ($p < 0.05$), and green indicates the decreased ones ($p < 0.05$). The neurons probed by Nissl staining (d), microglia recognized by Iba1 (e) and astrocytes recognized by GFAP (f) in brain slices (Scale bar = 500 μ m, n = 3 /group) were detected, and their numbers

This article is protected by copyright. All rights reserved.

were calculated (e, g, i). Data from the morphological analysis are presented as the means \pm SEM. * $p < 0.05$, ** $p < 0.01$, *** $p < 0.001$ versus SHAM.

Figure 4. Endoplasmic reticulum (ER) stress triggered apoptosis. In the differentially expressed proteins, some proteins related to cell death are listed with a ratio (OVX/SHAM, a) including Huntingtin-interacting protein K (HYPK), hexokinase (HK) and adenylate kinase 2 (AK2). Red color indicates the increased proteins ($p < 0.05$), and green indicates the decreased ones ($p < 0.05$). Levels of STIM2, glucose-regulated protein 78 (GRP78), protein kinase R (PKR)-like endoplasmic reticulum kinase (PERK), activating transcription factor 6 (ATF6), inositol-requiring enzyme-1 (IRE-1), eukaryotic initiation factor 2 α (EIF2 α), caspase-12 and cleaved caspase-12 (c-caspase-12) and the activity-related phosphorylation levels of PERK (p-PERK), IRE-1 (p-IRE-1) and EIF2 α (p-EIF2 α) in the HIP and AMY were assayed by Western blotting (b) and quantitative analysis (c, d) ($n = 6$ /group). Data are presented as the means \pm SEM. * $p < 0.05$, ** $p < 0.01$, *** $p < 0.001$ versus SHAM.

Figure 5. Autophagy activation and mitochondrial dysfunction triggered apoptosis. The differentially expressed proteins related to autophagy and mitochondria are listed with a ratio (OVX/SHAM, a) including γ -aminobutyric acid (GABA) receptor-associated protein-like 2 (GABARAPL2), autophagy-related 7 (ATG7), oxysterol-binding protein-related protein 1 (ORP1), heat shock 70 kDa protein 1A (HSPA1A), secretory carrier membrane protein 5 (SCAMP5), sideroflexin-1 (SFXN1), NADH dehydrogenase (ubiquinone) 1 α subcomplex 11 (NDUFA11), translocase of outer mitochondrial membrane 6 (TOMM6), mitochondrial import receptor subunit TOM34 (TOMM34), and mitochondrial import inner membrane translocase subunit (TIM16). Red color indicates the increased proteins ($p < 0.05$), and green indicates the decreased ones ($p < 0.05$). Levels of autophagy-related 5 (ATG5), microtubule-associated protein light chain 3 (LC3), Beclin1, B-cell lymphoma 2 (Bcl-2) and B-cell lymphoma 2 associated X (Bax), the phosphorylation levels of Bcl-2 (p-Bcl2) and p53 (p-p53), cytochrome c, and caspase-3 and cleaved caspase-3 (c-caspase-3) in the HIP and AMY were assayed by Western blotting (b) and quantitative analysis (c, d) ($n = 6$ /group). Data are presented as the means \pm SEM. * $p < 0.05$, ** $p < 0.01$, *** $p < 0.001$ versus SHAM.

Figure 6. Synaptic impairments and the imbalance of excitatory/inhibitory neurotransmission. The differentially expressed proteins related to synaptic impairments are listed with a ratio (OVX/SHAM, a) including Arf-GAP with SH3 domain, ANK repeat and PH domain-containing protein 1 (ASAP1), brain acid-soluble protein 1 (BASP1), septin-8 (SEPT8), vesicle-associated membrane protein 2 (VAMP2), calcium-dependent secretion activator 1 (CAPS1), *N*-methyl-D-aspartate receptor 2B (NR2B), metabotropic glutamate receptor 3 (mGluR3), mGluR4, vesicular glutamate transporter 1 (VgluT1), SH3, and multiple ankyrin repeat domains 3 (SHANK3), F-box only protein 2 (Fbxo2), Fyn, calretinin (CR), calbindin (CB), parvalbumin (PV) α , GABA type B receptor subunit 2 (GABAR-B2),

This article is protected by copyright. All rights reserved.

GABA transporter 3 (GAT3), GABA transporter 1 (GAT1), and hippocalcin-like protein 1 (HPCAL1). Red color indicates the increased proteins ($p < 0.05$), and green indicates the decreased ones ($p < 0.05$). Levels of postsynaptic density protein 95 (PSD95), synapsin1, synaptotagmin (Sty), glutamate receptor (GluR) 1 (GluR1), GluR2, NR1, NR2A, NR2B, α isoform of the calcium/calmodulin-dependent protein kinase II (CaMKII α), p-GluR1, TRPC1, protein kinase B (AKT) and the phosphorylation levels of CaMKII α (p-CaMKII α), NR-2B (p-NR2B) and AKT (p-AKT) in the HIP and AMY were assayed by Western blotting (b) and quantitative analysis (c, d) ($n = 6$ /group). To study alterations in the Ras/Raf1/mitogen-activated protein kinase kinase (MEK)/extracellular signal-regulated protein kinase (ERK) (Ras/Raf1/MEK/ERK) pathway, levels of Ras, Raf1, MEK, ERK and the phosphorylation levels of MEK (p-MEK) and ERK (p-ERK) in the HIP and AMY were assayed by Western blotting (e) and quantitative analysis (f, g) ($n = 6$ /group). Data are presented as the means \pm SEM. * $p < 0.05$, ** $p < 0.01$, *** $p < 0.001$ versus SHAM.

Figure 7. Impairments of the cytoskeleton in OVX rats. The differentially expressed proteins related to cytoskeletal impairments are listed with a ratio (OVX/SHAM, a) including microtubule-associated protein (MAP), tubulin α -1A chain (Tuba1a), α -tubulin N-acetyltransferase 1 (ATAT1), growth factor receptor-bound protein 2 (Grb2), Nudcd3, and phosphorylase b kinase (Phk). Red color indicates the increased proteins ($p < 0.05$), and green indicates the decreased ones ($p < 0.05$). Levels of total tau (Tau-5), dephosphorylated tau (Tau-1), and the phosphorylation of tau at Ser396 (pS396) and Ser404 (pS404), glycogen synthase kinase 3 β (GSK3 β), phosphorylated GSK3 β at Ser9 (p-GSK3 β), c-Jun-NH2-terminal kinase (JNK) and phosphorylated JNK at Thr183/Thr185 (p-JNK) in the HIP and AMY were assayed by Western blotting (b) and quantitative analysis (c, d) ($n = 6$ /group). Data are presented as the means \pm SEM. * $p < 0.05$, ** $p < 0.01$, *** $p < 0.001$ versus SHAM.

Table 1 Antibodies employed in this study and their properties

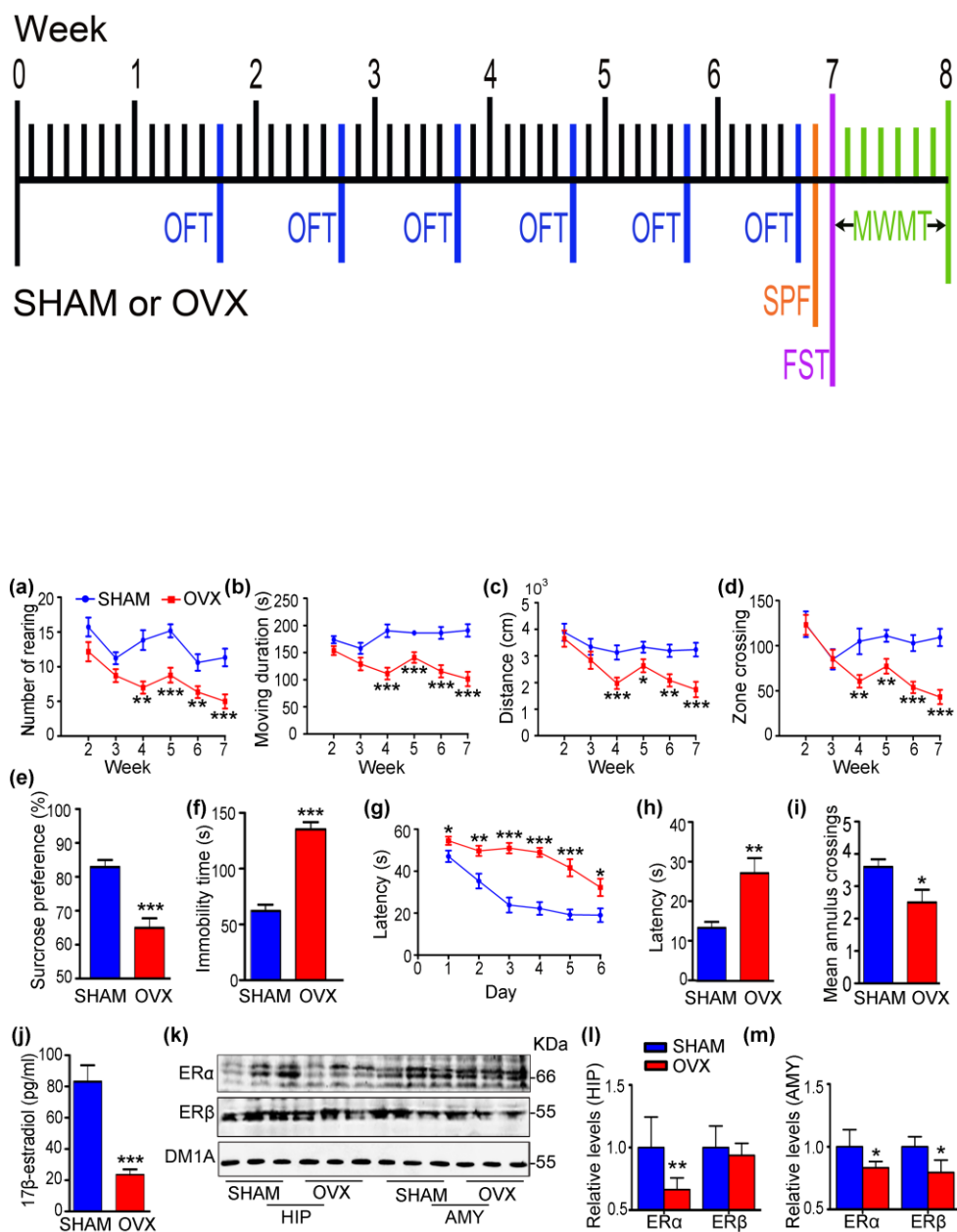
Antibody	Epitopes	mAb	Dilution	RRIDs	Catalogue numbers	Source
DM1A	α -tubulin	mAb	1:2000 (WB)	AB_2241126	ab7291	Abcam
ER α	Total ER α	pAb	1:500 (WB)	AB_631470	sc-542	Santa Cruz Biotechnology
ER β	Total ER β	pAb	1:1000 (WB)	AB_303922	ab3576	Abcam
Ras	Total Ras	pAb	1:1000 (WB)	AB_10695608	3965	Cell Signaling technology
Raf 1	Total Raf 1	mAb	1:1000 (WB)	AB_11213859	04-739	Millipore
MEK	Total MEK	pAb	1:1000 (WB)	AB_823567	9122	Cell Signaling technology
p-MEK	p-MEK at Ser217/221	mAb	1:1000 (WB)	AB_2138017	9154	Cell Signaling technology
ERK	Total MAPK ERK1/2	pAb	1:1000 (WB)	AB_390779	4695	Cell Signaling technology
p-ERK	p-ERK at Thr202/Tyr204	pAb	1:1000 (WB)	AB_2315112	4370	Cell Signaling technology
p-p53	p-p53 at Ser46	pAb	1:1000 (WB)	AB_10828689	2521	Cell Signaling technology
STIM2	Total STIM2	pAb	1:1000 (WB)	AB_10910274	4123	Prosci
TRPC1	Total TRPC1	pAb	1:200 (WB)	AB_477587	T8276	Sigma
GluR1	Total GluR1	pAb	1:1000 (WB)	AB_1977216	04-855	Millipore
p-GluR1	p-GluR1 at Ser845	pAb	1:1000 (WB)	AB_2533280	36-8300	Thermo Fisher scientific
GluR2	Total GluR2	mAb	1:1000 (WB)	AB_2113875	MAB397	Millipore
NR1	Total NR1	pAb	1:1000 (WB)	AB_2112158	AB9864	Millipore
NR2A	Total NR2A	pAb	1:1000 (WB)	AB_2112295	4205S	Cell Signaling technology
NR2B	Total NR2B	pAb	1:1000 (WB)	AB_1264223	4207S	Cell Signaling technology
p-NR2B	p-NR2B at Tyr1472	pAb	1:1000 (WB)	AB_304114	ab3856	Abcam
PSD95	Total PSD95	pAb	1:500 (WB)	AB_561221	2507	Cell Signaling technology

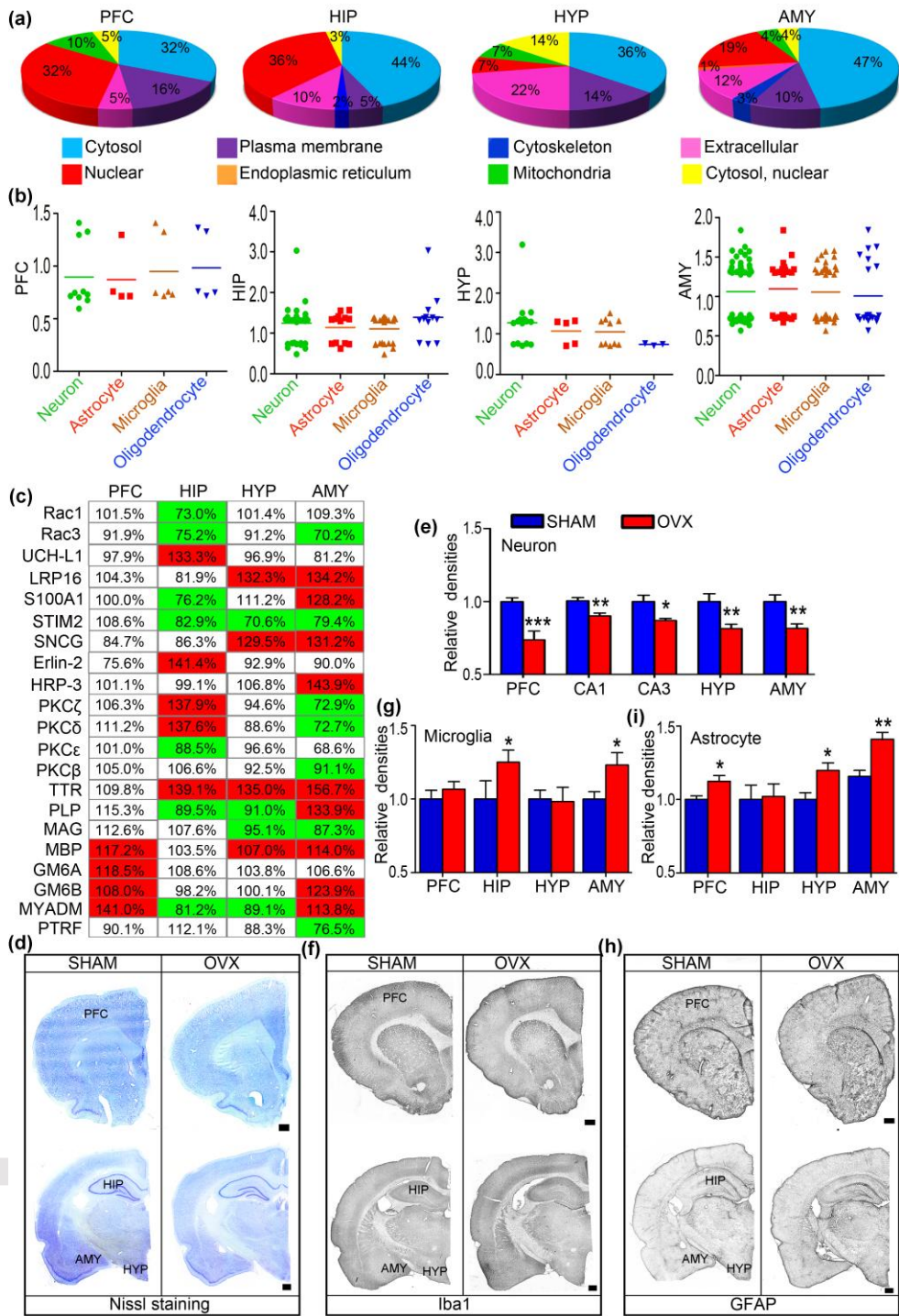
Synapsin 1	Total synapsin 1	pAb	1:1000 (WB)	AB_1281135	ab64581	Millipore
Synaptotagmin	Total synaptotagmin	mAb	1:1000 (WB)	AB_299799	ab13259	Abcam
Tau-5	Total tau	mAb	1:1000 (WB)	AB_1603723	ab80579	Abcam
Tau-1	dep-tau at Ser198/199/202	mAb	1:1000 (WB)	AB_94855	MAB3420	Millipore
pS396	p-tau at Ser396	mAb	1:1000 (WB)	AB_2266237	9632S	Cell Signaling technology
pS404	p-tau at Ser404	pAb	1:1000 (WB)	AB_896048	11112-2	Signalway Antibody
CaMKII α	Total CaMKII α	mAb	1:1000 (WB)	AB_325403	MA1-048	Thermo Fisher scientific
p-CaMKII α	p-CaMKII α at Thr 286	pAb	1:1000 (WB)	AB_2067915	sc-12886-R	Santa Cruz Biotechnology
Caspase-3	Total caspase-3	mAb	1:1000 (WB)	AB_2069872	9665S	Cell Signaling technology
Cleaved	Cleaved caspase-3	mAb	1:500 (WB)	AB_2070042	9664S	Cell Signaling technology
Caspase-12	Total caspase-12	pAb	1:500 (WB)	Cat. No.wl03000	wl03000	Wanleibio
Bcl2	Total Bcl2	pAb	1:1000 (WB)	AB_626736	sc-7382	Santa Cruz Biotechnology
p-Bcl2	p-Bcl2 at ser87	pAb	1:1000 (WB)	AB_2259052	sc-16323	Santa Cruz Biotechnology
Bax	Total Bax	pAb	1:1000 (WB)	AB_2064669	AB2915	Millipore
PERK	Total PERK	mAb	1:500 (WB)	AB_2095847	3192S	Cell Signaling technology
p-PERK	p-PERK at Thr980	mAb	1:500 (WB)	AB_2095853	3179S	Cell Signaling technology
EIF2 α	Total EIF2 α	mAb	1:500 (WB)	AB_836874	2103S	Cell Signaling technology
p-EIF2 α	p-EIF2 α at Ser51	pAb	1:500 (WB)	Cat. No. E-AB-20864	E-AB-20864	Enogene
ATF6	Total ATF6	pAb	1:1000 (WB)	AB_955682	ab62576	Abcam
GRP78	Total GRP78	pAb	1:1000 (WB)	AB_2119834	ab21685	Abcam
Cytochrome c	Total cytochrome c	mAb	1:1000WB)	AB_2090437	MAB897	R&D Systems
LC3	Total LC3	mAb	1:1000 (WB)	AB_2137707	3868S	Cell Signaling technology
Beclin 1	Total Beclin 1	pAb	1:1000 (WB)	AB_879596	ab55878	Abcam
ATG5	Total ATG 5	mAb	1:1000 (WB)	AB_2630393	12994	Cell Signaling technology

This article is protected by copyright. All rights reserved.

IRE-1	Total IRE-1	pAb	1:1000 (WB)	AB_775780	ab37073	Abcam
p-IRE-1	p-IRE-1 at Ser 724	pAb	1:1000 (WB)	AB_873899	ab48187	Abcam
JNK	Total SAPK/JNK	pAb	1:1000 (WB)	AB_632385	sc-571	Santa Cruz Biotechnology
p-JNK	p-JNK at Thr83/Tyr185	pAb	1:1000 (WB)	AB_331659	9251	Cell Signaling technology
AKT	Total AKT	pAb	1:1000 (WB)	AB_329827	9272	Cell Signaling technology
p-AKT	p-AKT at Ser 473	pAb	1:1000 (WB)	AB_331168	4058	Cell Signaling technology
GSK3 β	Total GSK3 β	pAb	1:1000 (WB)	AB_490890	9315S	Cell Signaling technology
p-GSK3 β	p-GSK3 β at Ser9	pAb	1:1000 (WB)	AB_2115201	9323	Cell Signaling technology
Iba-1	Total Iba-1	pAb	1:200 (IHC)	AB_839504	019-19741	Wako
GFAP	Total GFAP	mAb	1:100 (IHC)	AB_561049	3670	Cell Signaling technology

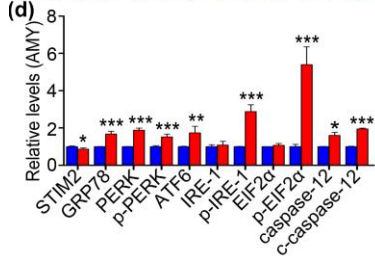
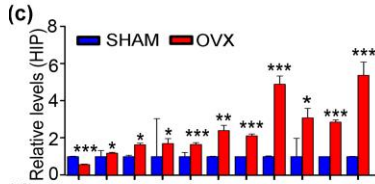
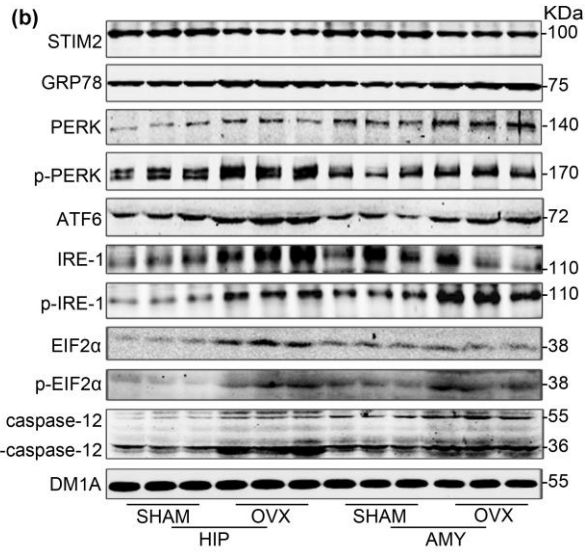
Key: p-, phosphorylated; mAb-, monoclonal antibody; pAb-, polyclonal antibody. WB, Western blot; IHC, Immunohistochemistry; RRIDs, Research Resource Identifiers.





(a)

	PFC	HIP	HYP	AMY
HYPK	83.6%	97.8%	96.9%	75.9%
HK	121.2%	85.8%	75.8%	137.2%
AK2	106.2%	79.6%	91.2%	134.8%



(a)

	PFC	HIP	HYP	AMY
GABARAPL2	113.1%	98.8%	106.4%	137.9%
ATG7	132.6%	136.4%	99.4%	114.2%
ORP1	87.3%	130.9%	94.3%	88.2%
HSPA1A	99.4%	98.0%	89.8%	76.3%
SCAMP5	106.5%	86.8%	135.9%	127.9%
SFXN1	108.2%	74.0%	106.5%	114.3%
NDUFA11	104.7%	87.2%	114.2%	131.9%
TOMM6	95.8%	48.3%	93.5%	83.1%
TOMM34	84.3%	104.3%	89.6%	70.8%
TIM16	109.9%	104.9%	81.4%	65.2%

